

High-Resolution Image Synthesis via Next-Token Prediction

Dengsheng Chen¹ Jie Hu^{1,2} Tiezhu Yue¹ Xiaoming Wei¹ Enhua Wu^{2*}

¹Meituan ²Key Laboratory of System Software (Chinese Academy of Sciences) and
State Key Laboratory of Computer Science, Institute of Software, Chinese Academy of Sciences

{chendengsheng, weixiaoming}@meituan.com, {hujie, weh}@ios.ac.cn

Abstract

*Recently, autoregressive models have demonstrated remarkable performance in class-conditional image generation. However, the application of next-token prediction to high-resolution text-to-image generation remains largely unexplored. In this paper, we introduce **D-JEPA-T2I**, an autoregressive model based on continuous tokens that incorporates innovations in both architecture and training strategy to generate high-quality, photorealistic images at arbitrary resolutions, up to 4K. Architecturally, we adopt the denoising joint embedding predictive architecture (D-JEPA) while leveraging a multimodal visual transformer to effectively integrate textual and visual features. Additionally, we introduce flow matching loss alongside the proposed Visual Rotary Positional Embedding (VoPE) to enable continuous resolution learning. In terms of training strategy, we propose a data feedback mechanism that dynamically adjusts the sampling procedure based on statistical analysis and an online learning critic model. This encourages the model to move beyond its comfort zone, reducing redundant training on well-mastered scenarios and compelling it to address more challenging cases with suboptimal generation quality. For the first time, we achieve state-of-the-art high-resolution image synthesis via next-token prediction.*

1. Introduction

In recent years, diffusion models have become the dominant approach for generating high-resolution images and videos from natural language inputs, demonstrating exceptional generalization capabilities [12–14, 28, 31, 35, 36, 41, 49, 55, 67, 70, 83, 90, 93, 95, 98, 100, 103, 106, 137]. At the same time, the rise of autoregressive large language models [1, 4, 5, 16, 26, 52, 61, 78, 85, 86, 88, 110, 113, 118, 119, 128, 129] has marked a new era in artificial intelligence, leading to significant advances in artificial general intelligence (AGI) due to their unparalleled versatility and

generality.

The success of language models has similarly catalyzed advancements in image generation [69, 89, 109, 130, 131]. Recent works, such as D-JEPA [20], MAR [64], and VAR [116], suggest that autoregressive models can achieve generative performance that rivals or even exceeds that of diffusion models in class-conditioned image synthesis on ImageNet [94]. However, despite their advantages in prompt adherence and computational efficiency over diffusion models [57], autoregressive models still face challenges in generating high-resolution images with fine-grained textures and overall visual fidelity.

To further advance autoregressive models for image generation and to foster the development of unified multi-modal models, we focus on two crucial aspects in this work: model architecture and training strategy.

From an **architectural perspective** (Sec. 2), we adopt the denoising joint embedding predictive architecture (D-JEPA) [20], building on its success in integrating representational learning to enhance model performance [134]. We also draw inspiration from the successful design principles of diffusion models, incorporating a multimodal visual transformer block, initially introduced by Esser et al., to ensure effective fusion of visual and textual features. Additionally, we leverage the more robust flow matching loss [70] to restore tokens into image patches. Furthermore, we identify that the conventional patchification operation, which segments continuous images into discrete blocks using RoPE [107], limits the model’s ability to handle continuous resolutions and varying aspect ratios. To address these challenges, we introduce the visual rotary positional embedding (VoPE), enabling the model to learn across continuous resolutions and dynamic aspect ratios.

In terms of **training strategy** (Sec. 3), we propose a novel data feedback mechanism to optimize resource efficiency. Traditional data curation typically involves pre-processing steps, such as filtering low-quality images [46] and refining prompts using multimodal models [65]. While these methods improve data quality, they often introduce biases and fail to adapt to evolving data distributions, particu-

*This work is supported in part by NSFC Grants (62332015).



Figure 1. D-JEPA·T2I can accurately generate high-fidelity, high-resolution images across various aspect ratios. Refer to the supplementary materials for 4K resolution samples and additional qualitative results.

larly in large-scale datasets. Fine-tuning techniques, such as reinforcement learning from human feedback (RLHF) [66, 126] and direct preference optimization (DPO) [87, 121], offer post-hoc adjustments but exhibit inconsistent effectiveness. In contrast, our data feedback mechanism dynamically adjusts the data distribution in real-time based on statistical analysis and model performance, as assessed by the critic model, during training. Specifically, the critic model is trained to evaluate the model’s performance on a sampled data point, providing continuous feedback to guide training.

By integrating the data-feedback training strategy into D-JEPA·T2I, we achieve state-of-the-art performance in high-resolution image synthesis via next-token prediction. Our approach has been validated on the T2I-CompBench [53], GenEval [42], and GenAI-Bench [63] benchmarks, as well as through human evaluations.

2. Model Architecture

The denoising joint embedding predictive architecture (D-JEPA) [20] builds upon the visual transformer [34] and models the token distribution $p(x_i|z_i)$, where z_i represents the predicted features of each token. It employs a combination of feature prediction loss $\mathcal{L}_{\text{pred}}$ and diffusion loss $\mathcal{L}_{\text{diff}}$. While D-JEPA has demonstrated strong performance in class-conditioned image generation, its applicability remains limited to fixed-resolution image synthesis, typically at 256×256 or 512×512 .

In this work, we introduce D-JEPA·T2I, extending D-JEPA to high-resolution text-to-image generation, as shown in Fig. 2. To achieve this, we adapt a multimodal visual transformer, building upon [36], to more effectively integrate textual and visual features (Sec. 2.1). Additionally, we replace the diffusion loss $\mathcal{L}_{\text{diff}}$ with a more flexible and

faster-converging flow matching loss $\mathcal{L}_{\text{flow}}$ (Sec. 2.2). Finally, we propose VoPE, a novel positional embedding for continuous-resolution learning (Sec. 2.3).

2.1. Multimodal Visual Transformer

The multimodal visual transformer draws inspiration from the design of the multimodal diffusion backbone, initially proposed by Esser et al. [36]. The core idea is that text and image embeddings are conceptually quite different, necessitating the use of two separate sets of weights for the two modalities. This approach is equivalent to having two independent transformers for each modality while concatenating their sequences for the attention operation. This setup allows both representations to operate within their own spaces while still incorporating information from the other.¹ Dehghani et al. [30] observe that the training of large vision transformer models diverges because the attention entropy grows uncontrollably. To avoid this, they propose normalizing Q and K before the attention operation. We follow this approach and use RMSNorm [135] with a learnable scale in both streams of D-JEPA·T2I architecture. The additional normalization prevents attention logit growth instability, confirming findings by previous works[30, 36, 124], and enables efficient training at bf16-mixed precision [19] when combined with the AdamW [72] optimizer.

The *primary distinction between the multimodal visual transformer and the multimodal diffusion backbone* is that the former does not require handling the additional timestep t introduced by the diffusion process. This omission sidesteps adaptive layer norm [82], which is essential for diffusion models built on top of DiT [80].

¹Refer to the supplementary materials for an illustration of the architecture.

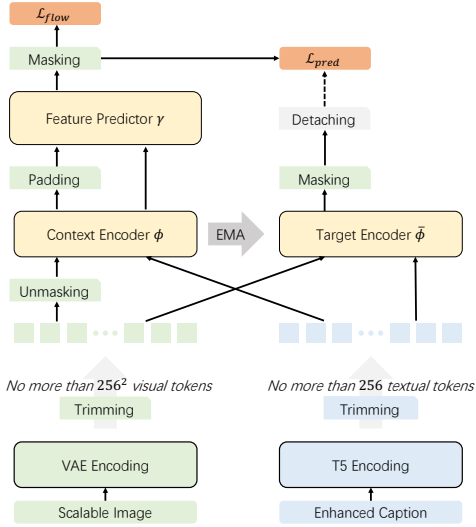


Figure 2. Denoising with a Joint-Embedding Predictive Architecture for text-to-image synthesis. We employ T5-XXL [27] as the text encoder, and the KL-VAE pretrained by Esser et al. [36] as the image encoder. Both textual and visual tokens are trimmed to no more than 256 and 256^2 tokens for efficient training, respectively. The feature predictor γ , the context encoder ϕ , and the target encoder $\bar{\phi}$ share the same network architecture, each consisting of several multimodal visual transformer blocks. The gradient is detached from the output of the target encoder $\bar{\phi}$, ensuring that it is only updated via exponential moving average (EMA). Both the prediction loss $\mathcal{L}_{\text{pred}}$ and the flow matching loss $\mathcal{L}_{\text{flow}}$ are computed only for the masked visual tokens, following Chen et al. [20].

For textual tokens, we follow the design principles of large language models and use RoPE [107] as positional encoding. For visual tokens, we introduce VoPE, a positional encoding specifically designed for visual features, which we detail in Sec. 2.3.

2.2. Flow Matching Loss

Flow matching [3, 67, 74, 76] emerges as a simple alternative that linearly interpolates between noise and data along a straight line. In this context, we adhere to the flow matching formulation presented in Gao et al. [41] for modeling the token distribution $p(x_i|z_i)$. More specifically, given the data $x_i \sim p(x_i|z_i)$ and Gaussian noise $\epsilon \sim \mathcal{N}(0, I)$, we define an interpolation-based forward process:

$$x_i^t = \alpha_t x_i + \beta_t \epsilon,$$

where $\alpha_0 = 0$, $\beta_0 = 1$, $\alpha_1 = 1$, and $\beta_1 = 0$. This interpolation for $t \in [0, 1]$ bridges $x_i^0 = \epsilon$ and $x_i^1 = x_i$. Similar to the diffusion schedule, this interpolation schedule offers flexible choices of α_t and β_t . In our framework, we adopt a linear interpolation schedule between noise and data for its simplicity: $x_i^t = tx_i + (1-t)\epsilon$. This formula-

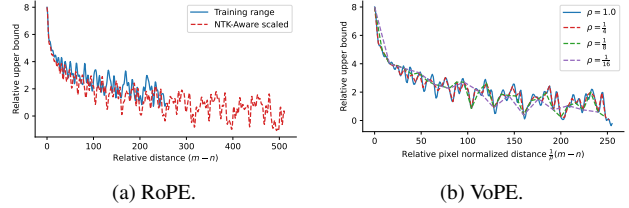


Figure 3. Comparison of decay curves between RoPE and VoPE.

tion represents a uniform transformation with constant velocity between the data and noise. The corresponding time-dependent velocity field is defined as:

$$v_t(x_i^t, z_i) = \dot{\alpha}_t x_i + \dot{\beta}_t \epsilon = x_i - \epsilon,$$

where $\dot{\alpha}$ and $\dot{\beta}$ denote the time derivatives of α and β . This time-dependent velocity field $v : [0, 1] \times \mathbb{R}^d \rightarrow \mathbb{R}^d$ defines an ordinary differential equation known as the Flow ODE:

$$dx_i = v_t(x_i^t, z_i) dt.$$

We use $\psi_t(x_i, z_i)$ to represent the solution of the Flow ODE with the initial condition $\psi_0(x_i, z_i) = x_i$. By solving this Flow ODE from $t = 0$ to $t = 1$, we transform noise into data samples using the approximated velocity fields $v_\theta(x_i^t, t, z_i)$. Similar to the approaches of Chen et al. [20] and Li et al. [64], v_θ is implemented with a small denoising MLP [64].

During training, the flow matching objective directly regresses to the target velocity for each token:

$$\mathcal{L}_{\text{flow}}(x_i, z_i) = \int_0^1 \mathbb{E} [\|v_\theta(x_i^t, t, z_i) - (x_i - \epsilon)\|^2] dt, \quad (1)$$

which is termed the conditional flow matching loss, sharing similarities with the noise prediction or score prediction losses in diffusion models [67].

2.3. VoPE for Continuous Resolution Learning

Empirically, autoregressive models face challenges when generating images with arbitrary resolutions and aspect ratios, mainly due to the absence of appropriate visual positional embeddings. Both sinusoidal positional encoding and rotary positional embedding have limitations: the former cannot ensure positional consistency when images are cropped or padded, and neither can maintain positional information consistency across different scales of the same image. Consequently, operations such as cropping, padding, or scaling an image can lead to models receiving completely different positional information if existing positional embedding schemes are applied directly.

These limitations significantly impact the learning of token distributions, potentially leading to flaws in generated high-resolution images. Here, we propose VoPE, a novel positional embedding for continuous resolution learning.

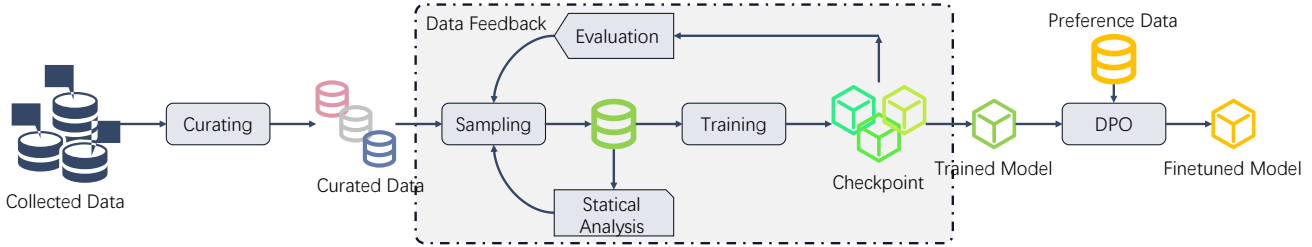


Figure 4. Training procedure incorporating data feedback. The evaluation result will be used to train the critic model.

Visual-rotary Positional Embedding. Visual-rotary positional embedding (VoPE) is inspired by biological vision and camera imaging principles. VoPE assumes that all objects are projected within a field of view with a fixed resolution of $g \times g$. For an image with resolution $W \times H$, any pixel at coordinate (w, h) can be normalized as:

$$\begin{cases} (\frac{1}{\rho}(w+b), \frac{1}{\rho}(h)), & W \leq H \\ (\frac{1}{\rho}(w), \frac{1}{\rho}(h+b)), & W > H \end{cases}$$

where $\rho = \max(W, H)/g$ is the resolution density, and $b = \text{abs}(W - H)/2$ is the relative positional offset. This normalization centers images on the grid $g \times g$, facilitating efficient learning from images of varying resolutions.

Consider a single row of tokens where q_m and k_n are tokens from query and key sequences, respectively. Su et al. [107] aim to implement relative positional encoding through absolute positional encodings with RoPE. VoPE targets the dot product between q_m and k_n to incorporate the relative positional information $\frac{1}{\rho}(m - n)$ while maintaining translation invariance. Thus, the inner product encodes positional information in a relative *pixel normalized* manner:

$$\langle f_q(x_m, \frac{1}{\rho}(m+b)), f_k(x_n, \frac{1}{\rho}(n+b)) \rangle = g(x_m, x_n, \frac{1}{\rho}(m-n)).$$

The aim is to determine an equivalent encoding mechanism for $f_q(x_m, \frac{1}{\rho}(m+b))$ and $f_k(x_n, \frac{1}{\rho}(n+b))$ that satisfies the above relation. Referring to Su et al. [107], the functions f and g that meet the relationship can be defined as follows when the feature dimension $d = 2$:

$$f_q(x_m, \frac{1}{\rho}(m+b)) = (\mathbf{W}_q x_m) e^{i[\frac{1}{\rho}(m+b)]\theta}$$

$$f_k(x_n, \frac{1}{\rho}(n+b)) = (\mathbf{W}_k x_n) e^{i[\frac{1}{\rho}(n+b)]\theta}$$

$$g(x_m, x_n, \frac{1}{\rho}(m-n)) = \text{Re}[(\mathbf{W}_q x_m)(\mathbf{W}_k x_n)^* e^{i[\frac{1}{\rho}(m-n)]\theta}],$$

where $\text{Re}[\cdot]$ denotes the real part, and $(\mathbf{W}_k x_n)^*$ is the complex conjugate of $(\mathbf{W}_k x_n)$. The constant $\theta \in \mathbb{R}$ is preset non-zero. When $d > 2$, $\theta_j = \omega^{-\frac{2(j-1)}{d}}$, $j \in [1, 2, \dots, d/2]$, where ω is a preset base frequency. For

larger d , the derivations and expressions of $f_q(x_m, \frac{1}{\rho}(m+b))$ and $f_k(x_n, \frac{1}{\rho}(n+b))$ are consistent with RoPE [107] and are not reiterated here.

Comparison between VoPE and RoPE. During sampling, RoPE requires adjusting the base frequency ω for higher resolution images. For instance, with a 256 token training length and a target of 512 tokens, the NTK-Aware Scaled RoPE approach [81] is used, where $\omega' = \frac{\omega}{2}$. Although effective for long texts, this causes discrepancies in positional information between training and sampling phases, as shown in Fig. 3a. These discrepancies are detrimental for image generation, which is sensitive to token boundary information. Gao et al. [41] noted that this method leads to blurry, repetitive images in higher resolution image generation, akin to issues in positional interpolation or extrapolation. Thus, RoPE is unsuitable for arbitrary resolution image generation, especially at higher resolutions. In contrast, VoPE ensures that pixel normalization maintains consistent positional information across resolutions during training and sampling. This is achieved by normalizing images to a $g \times g$ grid via ρ , without changing the base frequency ω , regardless of resolution. As shown in Fig. 3b, images at different resolutions with VoPE use the same relative positional curve at varying resolution densities ρ . Notably, at $\rho = 1/4$, the curve closely matches that of $\rho = 1.0$, implying that to generate 4096×4096 images, training at 1024×1024 with $\rho = 1/4$ suffices.² Beyond enabling different resolution image generation via ρ , VoPE allows layout adjustments in generated images with varying aspect ratios by adjusting the relative position bias b . Refer to the supplementary materials for further results.

2.4. High-resolution Image Sampling

For evaluating generative models in generalized next-token prediction, we employ an iterative sampling strategy similar to those used in Chang et al. [17], Li et al. [64], as outlined in Algo. 1. This strategy gradually decreases the masking ratio from 1.0 to 0.0 following a cosine schedule, typically using 64 autoregressive steps for sampling an image with a

²This assumes a VAE encoding stride of 8 and a patch size of 2.

resolution of 256×256 . Empirically, we find that even for higher-resolution images (such as 2K or 4K), satisfactory sampling quality can be achieved within approximately 100 autoregressive steps. D-JEPA-T2I follows the approach of Chen et al. [20], utilizing fully randomized orderings to determine the next set of tokens to predict. This design effectively enhances the diversity of the generated samples.

Algorithm 1 High-resolution image synthesis with D-JEPA-T2I in generalized next-token prediction.

Require: T : Number of auto-regressive steps, N : Total tokens to sample.

```

1: Initialize:  $\mathbb{X} \leftarrow \emptyset$ 
2: for  $n$  in cosine-step-function( $T, N$ ) do
3:    $\mathbb{C} \leftarrow \phi(\mathbb{X})$   $\triangleright$  Encode the sampled tokens
4:    $\mathbb{Z} \leftarrow \gamma(\mathbb{C})$   $\triangleright$  Predict features of unsampled tokens
5:    $\{z_0, \dots, z_n\} \sim \mathbb{Z}$   $\triangleright$  Randomly select  $n$  tokens
6:    $\{x_0, \dots, x_n\} \leftarrow \text{denoise}(\epsilon_\theta, \{z_0, \dots, z_n\})$ 
7:    $\mathbb{X} \leftarrow \mathbb{X} \cup \{x_0, \dots, x_n\}$   $\triangleright$  Add the denoised tokens
8: end for
9: Return:  $\mathbb{X}$ 

```

3. Training Strategy

While Esser et al. [36] and Li et al. [65] meticulously curate high-quality training data, they lack an in-depth examination of the actual sampled training data. To address this, we propose a statistical analysis and critic model sampling approach for more refined data selection. We refer to this novel training strategy as **data feedback**, and the training pipeline is depicted in Fig. 4.

3.1. Statistical Analysis Sampling.

It is worth noting that the curated training data does not always match the sampled training data and does not guarantee an optimal text-to-image model due to inherent data biases in natural distributions and the potential loss of long-tail data due to sampling. **(a) Data bias in natural distribution.** The distribution of training data obtained through curation rules typically presents significant biases. Since a large volume of training data is often sourced from publicly available internet data, the overall distribution, even post-curation, shows strong concentration regarding resolution and semantic notions.³ This can result in redundant data, thereby reducing the model’s overall performance. **(b) Under-sampling of long-tailed data.** Directly training with vast datasets (usually ranging from tens of millions to billions of image-text pairs) can potentially lead to the loss of long-tail data. In small-scale training, such as with ImageNet, the entire dataset is extensively traversed (e.g., thousands of iterations in Peebles and Xie [80]), providing the model ample opportunity to learn the distribution of all

³Please

training data. However, when the dataset scales up to billions, each data point might only be traversed a few times, and often the entire dataset might not be fully traversed even once. Resuming training typically recovers prior model parameters and optimizer states but struggles to track previously trained data indices, exacerbating the loss of long-tail data.

Statistical Analysis Sampling. To address these challenges, we perform statistical analysis on each batch of sampled data, examining features such as resolution, prompt composition, and style tags, and feed these features back into the sampling process for subsequent iterations in real-time. When sampling data, we introduce two distinct strategies to handle transformable and non-transformable attributes. *For transformable attributes* such as image resolution and aspect ratio, which can be adjusted without quality degradation, we utilize a truncated normal distribution sampling strategy, denoted as $\text{trunc_norm}(\mu, \sigma, a, b)$. We initially sample the desired data parameters, such as the target resolution. If the current data can be transformed to align with these specified parameters, we proceed with the transformed data; otherwise, we discard this sample and attempt resampling. In contrast, *for non-transformable attributes*, we decide whether to use the current data based on a predetermined sampling frequency specific to each attribute. If the data exceeds this frequency, there is a 50% probability it will be discarded. Although this approach may not strictly adhere to the exact predetermined sampling frequencies, it significantly enhances data utilization, particularly beneficial when dealing with the sampling of long-tail distributions.

Based on statistical analysis sampling, we can achieve a more reliable and balanced selection, ensuring uniform sampling of all data types as expected.

3.2. Critic Model Sampling

Does uniformly sampling all types of data necessarily lead to a well-trained generative model? The answer is clearly no. While diverse data distribution ensures a broad representation within the dataset, diversity alone is merely a fundamental prerequisite for training a model with general capabilities. Critic model sampling is designed to address the inherent weaknesses of the model during the training process.

In the early training stages, we employ statistical analysis sampling to expose the model to a wide variety of data, helping it establish a foundational knowledge system. However, in practice, we observe that the model quickly learns to generate certain types of content while struggling with others. Some types of data may take significantly longer to learn, or in some cases, the model may never master them. Critic model sampling aims to identify the types of content

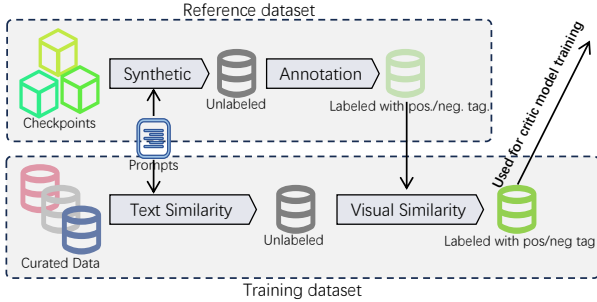


Figure 5. The pipeline to prepare training set for critic model.

that the model finds challenging and prioritize them during training. By doing so, we continuously refine the model’s abilities and mitigate its weaknesses.

A key aspect of this approach involves the online learning of the critic model. As illustrated in Fig. 5, we follow a structured pipeline for training the critic model. **(a) Data preparation.** First, we collect a sufficiently large set of prompts that cover a comprehensive range of scenarios (typically in the thousands). Next, we load the current T2I model weights and generate a substantial number of synthetic images for each prompt to form a reference set. Additionally, we retrieve several images from the training dataset based on text similarity with each prompt to construct the training set. **(b) Data annotation.** *For the reference set*, in the early training stages—when the model’s performance is still suboptimal—we utilize automated evaluation metrics such as T2I CompBench [53] to assess whether generated images meet the fundamental requirements of the prompts. Images that meet the criteria are labeled as positive samples, while those that fail are labeled as negative samples. As training progresses and the model’s output quality improves, we introduce human evaluation. At this stage, experts assess each generated image from a professional photography perspective, considering aspects such as logical consistency and realism. Images that meet the quality criteria are labeled as positive samples, while those that do not are marked as negative. *For the training set*, after completing the reference set annotations, we compute the feature similarity between images in the training set and their corresponding reference set images. Images with high feature similarity inherit the reference set labels, while those with low similarity are discarded. Since the model is still relatively weak in the early stages, we adopt a lower similarity threshold for automatically labeled reference images. In later stages, when human annotations are available, we raise the threshold to ensure a sufficiently large and high-quality training dataset. **(c) Training the critic model.** We employ a ResNet-18 model [44], modifying it into a binary classification network. For the first round of critic model training, we initialize it with ImageNet pre-trained weights collected by [Wightman](#). In subsequent updates, we use the previous

version of the critic model as the initialization. Since the T2I model continuously evolves, the critic model must also be updated accordingly. In our implementation, we introduce critic model sampling after the first 100K iterations of the T2I model. Thereafter, we update the critic model every 40K iterations. The training process follows standard ImageNet classification strategies and data augmentation techniques [123]. Given that the dataset consists of tens of thousands of samples, the computational overhead of training the critic model is negligible.

Critic Model Sampling. Once training is complete, we validate the samples obtained from statistical analysis sampling. The critic model assigns each sample a probability of being rejected (*i.e.*, the likelihood that the model struggles with this type of content). Since we aim to sample more challenging cases where the model performs poorly, a higher rejection probability indicates that the model handles the sample well and should be discarded. Conversely, lower-probability samples are prioritized for training.

Comparison between critic model sampling and fine-tuning techniques. Fine-tuning techniques, such as reinforcement learning from human feedback (RLHF) [66, 126] and direct preference optimization (DPO) [87, 121], provide post-hoc adjustments but often exhibit inconsistent effectiveness. Our proposed critic model sampling can be seen as an online counterpart to fine-tuning techniques. Moreover, the utilization of human annotation data differs between these approaches. In the fine-tuning stage, human annotators typically collect a new source of high-quality training data to directly improve the T2I model. In contrast, critic model sampling requires only a few thousand synthetic images to be annotated with positive and negative labels, which are then used solely for training the critic model—without necessitating additional new training data sources. In summary, critic model sampling focuses on improving the utilization of existing data, whereas fine-tuning techniques emphasize incorporating new data sources to enhance model performance.

4. Experiments

In this section, we succinctly outline the experimental configuration and training process of D-JEPA-T2I. We evaluate the model performance through automated metrics, qualitative results, and human ratings. *Detailed experimental setups and crucial ablation studies (concerning VoPE, data feedback, and more) are provided in the supplementary material.*

VQAScores on “basic” prompts						
Method	Attribute	Scene	Spatial	Action	Part	Avg
SD v2.1 [93]	0.75	0.79	0.73	0.73	0.71	0.75
SD-XL Turbo [96]	0.81	0.82	0.78	0.79	0.78	0.80
SD-XL [83]	0.82	0.85	0.80	0.80	0.81	0.82
DeepFloyd-IF [40]	0.82	0.83	0.80	0.81	0.81	0.82
SD3.0 medium [36]	0.88	0.88	0.88	0.87	0.89	0.88
D-JEPA-T2I	0.84	0.86	0.86	0.85	0.82	0.84
Midjourney v6 [75]	0.86	0.88	0.86	0.87	0.85	0.86
DALL-E 3 [12]	0.91	0.91	0.90	0.90	0.91	0.90
VQAScore on “advanced” prompts						
Method	Count	Differ	Compare	Negate	Universal	Avg
SD v2.1 [93]	0.66	0.64	0.65	0.51	0.63	0.60
SD-XL Turbo [96]	0.71	0.68	0.69	0.52	0.66	0.63
SD-XL [83]	0.72	0.70	0.69	0.50	0.67	0.63
DeepFloyd-IF [40]	0.70	0.70	0.71	0.50	0.65	0.63
SD3.0 medium [36]	0.75	0.77	0.73	0.47	0.70	0.65
D-JEPA-T2I	0.76	0.75	0.72	0.49	0.72	0.66
Midjourney v6 [75]	0.77	0.77	0.76	0.50	0.73	0.68
DALL-E 3 [12]	0.80	0.80	0.77	0.49	0.75	0.69

Table 1. VQAScores on “basic” and “advanced” prompts assessed by GenAI-Bench [63].

4.1. Experiment Setup

Dataset. We employ an internally curated dataset comprising over 1 billion image-text pairs for training. Each image has a minimum shorter side length of 512 pixels. To maintain high quality, images with aesthetic scores below 5.0 are excluded using the LAION-AI aesthetic predictor⁴. Additionally, OCR tools filter out images containing text, which constrains the model from generating text but enhances its learning of other real-world concepts. English captions are generated for each image using InternVL2 [24, 25], and enhanced with image tags (e.g., style tags, data source). Synthetic datasets, like JourneyDB [108], are carefully incorporated despite their efficacy in accelerating convergence [21, 41]. We hypothesize that over-dependence on synthetic data might limit the model’s output diversity, reducing data utility. Thus, synthetic data constitutes only about 5% of the dataset, ensuring D-JEPA-T2I generates authentic content, albeit with slower convergence.

Training. The D-JEPA-T2I model extends D-JEPA-H [20] and comprises 2.6 billion parameters. Training is strategically divided into two phases. *Initially*, the model is trained on images no larger than 256×256 pixels⁵, using a batch size of 2048 for 100k steps, with only statistical analysis sampling applied. This phase is crucial for enhancing textual concept comprehension. A cosine annealing schedule is employed, adjusting the learning rate from 1×10^{-5} to 1×10^{-6} , with a warm-up of 10k steps. *In the second phase*, the model trains on diverse image scales and resolutions, with batch sizes dynamically adjusted based on sampled resolutions from a truncated normal distribution (see Para. 3.1). Image resolutions progressively increase from

⁴github.com/LAION-AI/aesthetic-predictor

⁵For images with resolutions greater than 256×256 , we apply aspect ratio-preserving resizing.

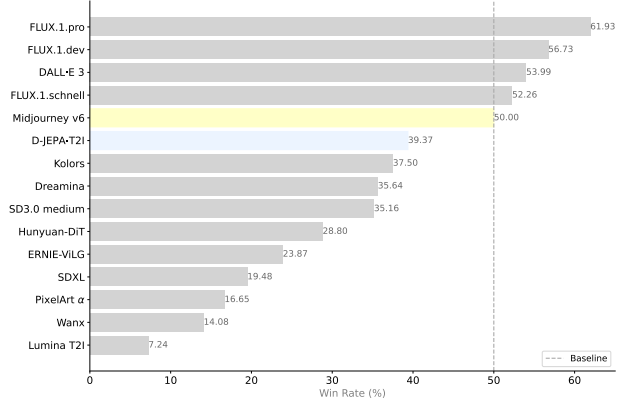


Figure 6. Models’ win rate against Midjourney v6 [75]. The evaluated models include Kolors [114], Dreamina [112], ERNIE-ViLG [38], and Wanx [115].

128 to 1024 pixels over the subsequent 500k iterations. Refer to the *supplementary material* for more details on resolution sampling. During this phase, critic model sampling is introduced and updated every 40k iterations.

Empirically, we find that with statistical analysis sampling alone, the model achieves an overall score of 0.50 on GenEval within 100k training steps, matching the performance of SD2.0 [93] and PixArt- α [21]. After introducing the critic model, trained with the automated evaluation-based trick, the model approaches its final performance at 200k steps, showing gradual improvement between 200k and 300k steps, ultimately reaching 0.66—surpassing models of comparable scale. In the final 300k training steps, the reference set is labeled via human evaluation. While this stage does not significantly improve performance on standard benchmarks like GenEval [42], it leads to substantial advancements in image realism and photographic style, as reflected in human ratings, which increased from a win rate of less than 20% against Midjourney v6 to over 30%.

The full training process was conducted on 128 H800 GPUs over two weeks. The reference set required for updating the critic model was constructed using two different approaches based on the annotation method. During the automated annotation phase (100k–300k steps), we generated approximately 100k images at 256×256 resolution, as this stage primarily targets fundamental model capabilities. Since automated annotation mainly detects the presence of corresponding concepts, generating low-resolution images not only reduces inference time but also ensures comprehensive model evaluation. In the later stage (300k–600k steps), we generated around 10k images at resolutions ranging from 512 to 1024 pixels. At this point, the model had already acquired strong generative abilities, allowing human annotators to conduct meticulous evaluations and enforce stricter selection criteria, further driving model optimization.

Model	NTP	#Params	GenEval							T2I-CompBench++		
			Overall	Single Obj.	Two Obj.	Counting	Colors	Position	Color Attr.	Color	Shape	Texture
SD 3.0 [36]	×	2.0B	0.62	0.98	0.74	0.63	0.67	0.34	0.36	0.8132	0.5885	0.7334
D-JEPA-T2I	✓	2.6B	0.66	0.99	0.80	0.59	0.87	0.22	0.47	0.7585	0.5036	0.6355
SDXL [83]	×	2.6B	0.55	0.98	0.74	0.39	0.85	0.15	0.23	0.5879	0.4687	0.5299
LlamaGen [109]	✓	3.1B	0.32	0.71	0.34	0.21	0.58	0.07	0.04	-	-	-
SD 3.0 [36]	×	4.0B	0.64	0.96	0.80	0.65	0.73	0.33	0.37	-	-	-
SD 3.0 [36]	×	8.0B	0.68	0.98	0.84	0.66	0.74	0.40	0.43	-	-	-
Emu3 [122]	✓	8.0B	0.54	0.98	0.71	0.34	0.81	0.17	0.21	-	-	-
Fluid [37]	✓	10.5B	0.69	0.96	0.83	0.63	0.80	0.39	0.51	-	-	-
DALL-E 3 [12]	×	-	0.67	0.96	0.87	0.47	0.83	0.43	0.45	0.7785	0.6205	0.7036
Midjourney v6 [75]	×	-	0.63	0.96	0.81	0.56	0.83	0.22	0.42	0.7503	0.6885	0.6101

Table 2. Comprehensive comparison with state-of-the-art models on the GenEval [42] and T2I CompBench++ [53] benchmarks. All listed metrics are obtained without employing DPO or prompt rewriting techniques. The symbol ✓ denotes the use of the Next Token Prediction (NTP) strategy for image sampling. DALL-E 3 [12] and Midjourney v6 [75] are commercial closed-source models, and their exact model sizes are not publicly available. A complete table is provided in the supplementary material.

Before conducting the final evaluation on human rating, we performed direct preference optimization (DPO) training. This training utilized an additional ultra-high-quality dataset and was conducted for 20k steps. The primary objective of this stage was to refine the model’s image style and texture, making them more closely resemble real photographic aesthetics. Notably, we did not attempt to enhance other aspects of the model, such as text generation quality.

Inference. The D-JEPA-T2I model can generate images at arbitrary resolutions and aspect ratios. For 256×256 resolution images used in quantitative evaluation, we set autoregressive steps to $T = 64$. For higher resolutions, autoregressive steps are empirically tuned. Classifier-free guidance [47] enhances image quality, with hyperparameters optimized per benchmark. Denosing MLP diffusion steps are consistently set to 250 across tasks.

4.2. Automated Metric Evaluation

We evaluate our method using automated metrics on prominent text-to-image benchmarks, including GenEval [42], T2I-CompBench [53], and GenAI-Bench [63], which assess the model’s capacity to generate prompt-reflective images. Table 2 compares D-JEPA-T2I against state-of-the-art diffusion and autoregressive models, both open-source and closed-source. The number of model parameters significantly influences performance; thus, comparisons among similar-scale models offer practical insights.

Per GenEval overall scores in Tab. 2, D-JEPA-T2I surpasses other models within small and mainstream sizes. Compared with larger models, D-JEPA-T2I (2.6B parameters) excels over Emu3 [122] (8.0B) and Transfusion (7.3B), and is competitive with Fluid (10.5B). It also rivals commercial models like DALL-E 3 [12] and Midjourney v6 [75].

Regarding T2I-CompBench++, D-JEPA-T2I outperforms previous open-source works like PixArt- α [21] and SDXL [83], achieving a pioneering level in the field. In Tab. 1, D-JEPA-T2I surpasses SD 3.0 [36] in advanced

prompt generation, maintaining a leading position. These findings robustly demonstrate that as an autoregressive model, D-JEPA-T2I has achieved state-of-the-art performance in text-to-image tasks for the first time, exhibiting substantial potential.

4.3. Qualitative Results

Fig. 1 illustrates the versatile capabilities of images generated by D-JEPA-T2I, which supports flexible resolutions and aspect ratios and can adeptly handle various styles. ⁶

4.4. Human Ratings

We selected 532 challenging and representative prompts from GenEval [42], T2I-CompBench [53], PickScore [59], and Parti-prompts [131] to construct a comprehensive human evaluation benchmark. This benchmark assesses generated images based on prompt adherence, coherence, and realism.

To facilitate method comparison, we use Midjourney v6 [75] as a baseline. Models are compared pairwise with Midjourney v6. The win rate in Fig. 6 shows that D-JEPA-T2I outperforms the diffusion model SD3.0 medium [36] and performs comparably to Midjourney v6. Although D-JEPA-T2I currently trails behind the FLUX series and DALL-E 3, it’s notable that FLUX has 12B parameters, markedly larger than our model’s 2.6B scale. As for DALL-E 3, being a closed-source commercial model, its exact parameter count is unknown but inferred to surpass 2.6B based on DALL-E 2’s 4.2B.

5. Conclusion

In this work, we introduce D-JEPA-T2I, along with the VoPE positional encoding and a data feedback training strategy, aimed at enhancing the capability of autoregressive models to generate high-resolution images. Our empirical results demonstrate comprehensive outperformance over both diffusion models and existing autoregressive models

⁶Refer to the supplementary material for more qualitative results.

in the text-to-image generation task. Future research will delve into further validation of scaling laws on D-JEPA-T2I and investigate the effective application of the D-JEPA architecture to video generation, as well as building a unified multimodal model.

High-Resolution Image Synthesis via Next-Token Prediction

Supplementary Material

6. Additional Figures and Tables

Teaser. Fig. 7 presents the complete teaser image.

Distribution. Fig. 8 illustrates the issue of uneven natural data distribution.

D-JEPA-T2I. Fig. 9 provides a detailed overview of the full network architecture.

Full Table. Tab. 3 lists the complete comparison results.

7. Related Work

Diffusion Models. The pioneering work of Ho et al. [49], Sohl-Dickstein et al. [99], Song et al. [105] established a methodology for data generation by approximating the reverse ordinary differential equation of a stochastic forward process that transforms data into noise. This novel approach has become a cornerstone in both image [6, 31, 90, 93, 95] and video generation domains [14, 35, 43, 50, 98].

Expanding on derivations based on the variational lower bound on negative likelihood [99] and score matching [54, 104, 120], researchers have explored various formulations of forward and reverse processes [32, 105], model parameterizations [47, 49, 55], loss weightings [49, 55], and ODE solvers [33, 73, 101]. Significant contributions by Kingma and Gao [58] and Karras et al. [55] have provided unified formulations that offer novel theoretical and practical insights for both training [55, 58] and inference [55]. Nonetheless, common ODE trajectories often exhibit significant curvature [55, 70], requiring numerous solver steps and complicating rapid inference.

Recent research efforts have aimed at improving learning and sampling methods [7, 73, 100, 103], utilizing guidance techniques [47, 77], leveraging latent learning [93], and advancing architectural designs [51, 80, 95, 127]. Innovative models like DiT [80] and U-ViT [8] integrate or replace the U-Net with transformers, inspiring advancements in image [21, 22] and video synthesis systems [11, 43], including Stable Diffusion 3.0 [36], SORA [15], and Vidu [9].

Rectified Flow Models. Rectified flow models [2, 68, 70] approach generative modeling by constructing a transport map between two distributions via an ordinary differential equation (ODE). This technique is closely related to continuous normalizing flows (CNF) [23] and diffusion models. Compared to CNFs, rectified flows and stochastic interpolants eliminate the need for ODE simulation during

training. Compared to diffusion models, they can generate ODEs that are faster to simulate than the probability flow ODE [105] associated with diffusion models. However, rectified flow models do not yield optimal transport solutions, which has led to efforts aiming to minimize trajectory curvature [62, 84, 117]. Recent works [29, 74] demonstrate the feasibility of rectified flow formulations for class-conditional image synthesis, while Fischer et al. [39] employs them for latent-space upsampling, and Liu et al. [71] leverages the reflow procedure from [70] to distill a pre-trained text-to-image model [93]. In this study, we focus specifically on employing rectified flows as the flow matching loss to effectively model the distribution of each token.

Masked Prediction Models. MaskGIT [17] utilizes a vector-quantized autoencoder [92] along with a masked prediction transformer similar to BERT [10, 45, 56] to generate discrete tokens via a greedy algorithm. This approach is extended to videos by MagViT [132], and further refined by MagViT-2 [133], which enhances these techniques [17, 132] with an improved VQ-VAE [92] for both images and videos. MUSE [18] scales MaskGIT to 3 billion parameters. Recent developments by Chen et al. [20], Li et al. [64], Tian et al. [116] have shifted away from reliance on VQ-VAE, opting instead for KL-VAE, yielding better results. Despite these advancements, masked prediction models (or autoregressive models) still lag behind diffusion models and rectified flow models in the context of high-resolution text-to-image generation tasks.

8. Data Processing

To obtain high-quality image-text pairs and mitigate data bias, we performed a comprehensive analysis of the dataset to achieve a more balanced distribution of training data.

Beyond conventional filters such as resolution, OCR [102], face detection⁷, aesthetic score⁸ and NSFW content⁹, we examined the distribution of basic information for every data source and the distribution among different feature combinations, such as resolution and aspect ratio. This approach enabled us to identify the fundamental characteristics of the different datasets.

Our analysis focused on the distribution of entity words and attribute words in the captions obtained using In-

⁷<https://huggingface.co/arnabdhar/YOLOv8-Face-Detection>

⁸<https://github.com/LAION-AI/aesthetic-predictor>

⁹<https://github.com/LAION-AI/CLIP-based-NSFW-Detector>

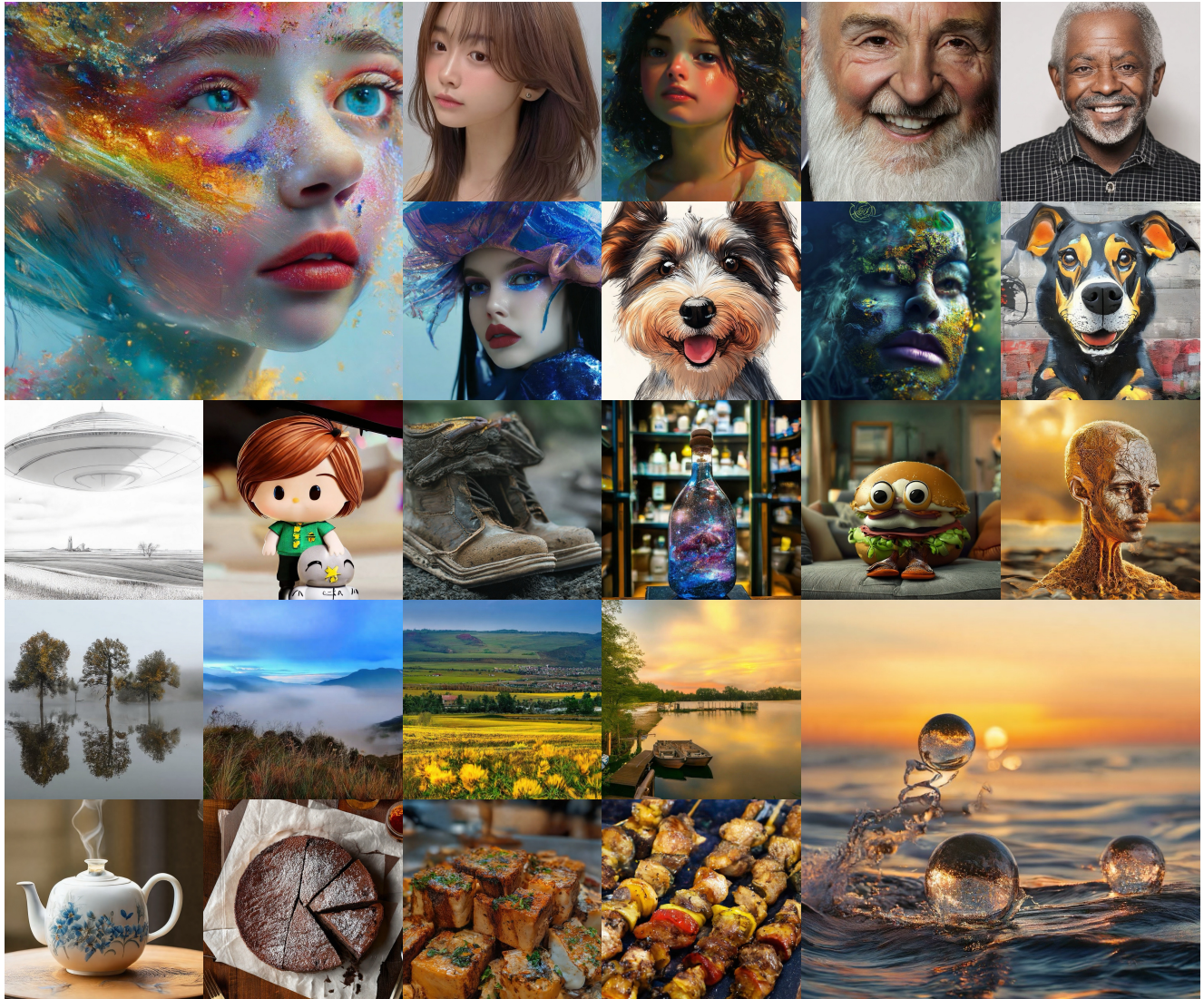


Figure 7. 1K-resolution images sampled from D-JEPA-T2I, showcasing its ability to generate high-fidelity, high-resolution images. (Best viewed when zoomed in.)

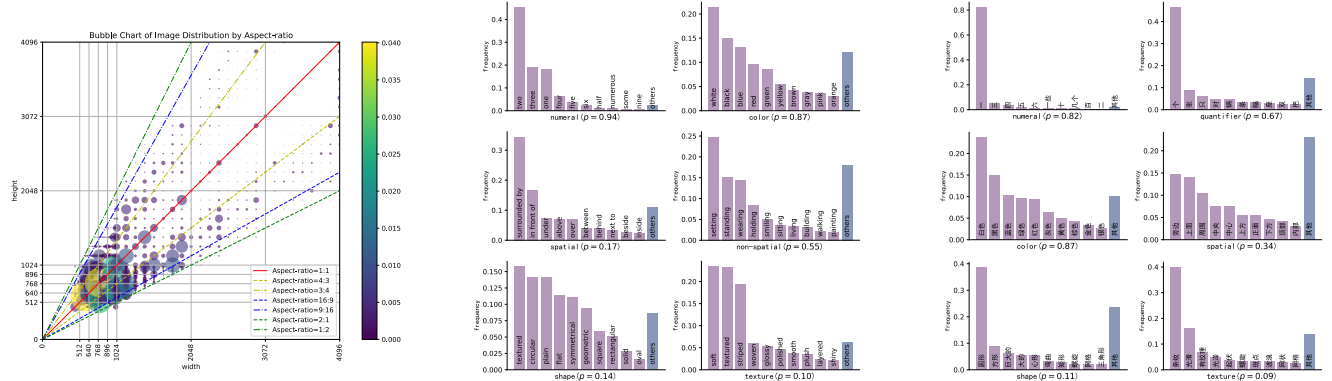
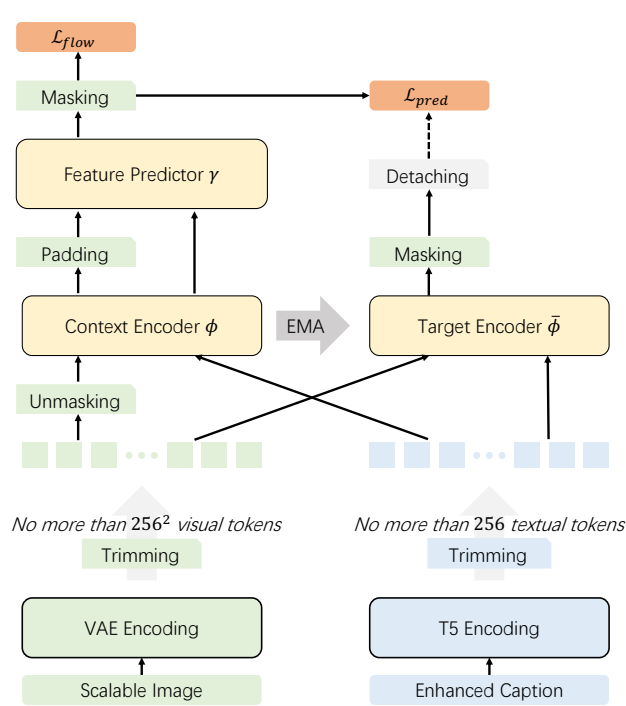
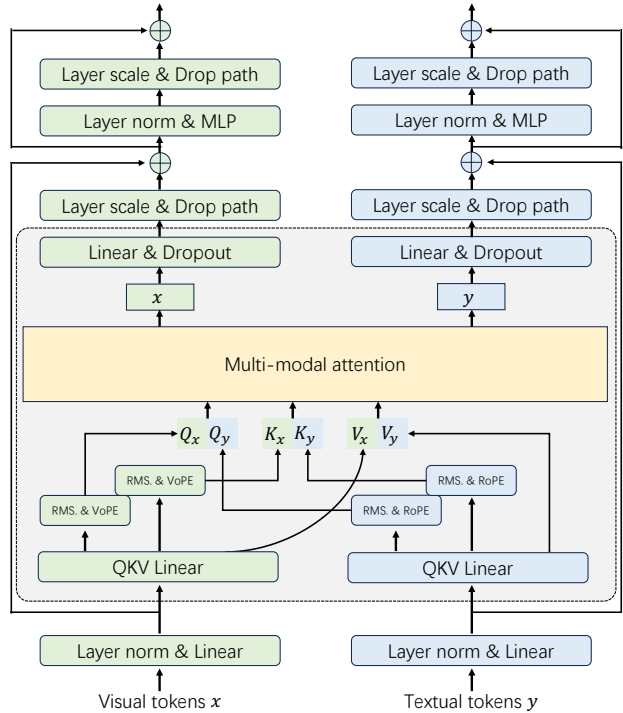


Figure 8. The resolution and notion distribution in the curated LAION dataset [97], where p represents the proportion of prompts containing a given notion. Additionally, we plot the distribution of translated Chinese characters in the third subplot as a supplementary reference, highlighting that the observed distribution imbalance is inherent to the dataset itself rather than being language-dependent.



(a) Overview of all components.



(b) Multi-modal visual transformer block.

Figure 9. Denoising with a Joint-Embedding Predictive Architecture for text-to-image synthesis. We present the overview of D-JEPA-T2I in Fig. 9a. We employ T5-XXL [27] as the text encoder, and the KL-VAE pretrained by Esser et al. [36] as the image encoder. Both textual and visual tokens are trimmed to no more than 256 and 256^2 tokens for efficient training, respectively. The feature predictor γ , the context encoder ϕ , and the target encoder $\bar{\phi}$ share the same network architecture, each consisting of several multimodal visual transformer blocks, as illustrated in Fig. 9b. The gradient is detached from the output of the target encoder $\bar{\phi}$, ensuring that it is only updated via Exponential Moving Average (EMA). Both the prediction loss $\mathcal{L}_{\text{pred}}$ and the flow matching loss $\mathcal{L}_{\text{flow}}$ are computed only for the masked visual tokens, following Chen et al. [20].

ternVL2 [24]. Utilizing standard NLP tools¹⁰, we extracted entity words, including abstract concepts, from the captions. The attribute words primarily included numerals, quantifiers (specific to Chinese), spatial terms, non-spatial terms (specific to English), shapes, colors, and textures, in conjunction with metrics from T2I-CompBench [79] and GenEval [42]. Initially, we obtained a comprehensive vocabulary list for specific attributes using GPT-4 [1]. The prompt was: “Please return as many words as possible that describe numerals/colors/shapes/positions/textures in English/Chinese. Directly return the list result [], DO NOT hallucinate, and avoid polite language.” For non-spatial terms, we referred to the 1000 prompts provided in T2I-CompBench¹¹ to analyze the gerunds. We then employed regular expressions to match these words in the captions and counted their frequency of occurrence, prioritizing longer attribute words during the matching process.

¹⁰<https://github.com/explosion/spaCy>

¹¹https://github.com/Karine-Huang/T2I-CompBench/blob/main/examples/dataset/non_spatial.txt

9. Experiments Details

Scaling to 4K Resolution. To support 4K resolution image generation, we need to resolve two main issues. First, high-resolution images can lead to insufficient GPU memory during VAE encoding and decoding. Second, the token sequences corresponding to high-resolution images are considerably lengthy, resulting in memory limitations during training. Common engineering solutions involve using Zero Redundancy Optimizer [91] and Megatron¹² to offload some optimizer states to the CPU, or employing strategies like model parallelism and tensor parallelism.

Here, we devise a data-efficient training technique to enable training at 4K resolution and beyond with D-JEPA-T2I. Unlike diffusion models, which require processing entire images per iteration, the autoregressive D-JEPA-T2I can predict random portions of images based on random context tokens. Thus, when the total number of tokens exceeds 4096 (i.e., 256 tokens per side), we apply a random drop strategy to maintain the token count at 4096 or

¹²<https://github.com/NVIDIA/Megatron-LM>

Model	NTP	#Params	GenEval							T2I-CompBench++		
			Overall	Single Obj.	Two Obj.	Counting	Colors	Position	Color Attr.	Color	Shape	Texture
<i>Small model size</i>												
PixArt- α [21]	×	0.6B	0.48	0.98	0.50	0.44	0.80	0.08	0.07	0.4232	0.3764	0.4808
SD v1.x [93]	×	0.9B	0.43	0.97	0.38	0.35	0.76	0.04	0.06	0.3765	0.3576	0.4156
SD v2.x [93]	×	0.9B	0.50	0.98	0.51	0.44	0.85	0.07	0.17	0.5065	0.4221	0.4922
SD 3.0 [36]	×	1.0B	0.58	0.97	0.72	0.52	0.78	0.16	0.34	-	-	-
Show-o [125]	✓	1.3B	0.53	0.95	0.52	0.49	0.82	0.11	0.28	-	-	-
LDM [93]	×	1.4B	0.37	0.92	0.29	0.23	0.70	0.02	0.05	-	-	-
Hunyuan-DiT [65]	×	1.5B	0.57	0.96	0.67	0.59	0.83	0.11	0.26	0.6565	0.3577	0.4718
<i>Mainstream model size</i>												
Lumina-T2I [137]	×	2.0B	0.39	0.88	0.34	0.31	0.67	0.05	0.09	0.4081	0.3008	0.4071
SD 3.0 [36]	×	2.0B	0.62	0.98	0.74	0.63	0.67	0.34	0.36	0.8132	0.5885	0.7334
D-JEPA-T2I	✓	2.6B	0.66	0.99	0.80	0.59	0.87	0.22	0.47	0.7585	0.5036	0.6355
SDXL [83]	×	2.6B	0.55	0.98	0.74	0.39	0.85	0.15	0.23	0.5879	0.4687	0.5299
LlamaGen [109]	✓	3.1B	0.32	0.71	0.34	0.21	0.58	0.07	0.04	-	-	-
SD 3.0 [36]	×	4.0B	0.64	0.96	0.80	0.65	0.73	0.33	0.37	-	-	-
DALL-E 2 [90]	×	4.2B	0.52	0.94	0.66	0.49	0.77	0.10	0.19	-	-	-
<i>Extensive model size</i>												
Chameleon [111]	✓	7.0B	0.39	-	-	-	-	-	-	-	-	-
Transfusion [136]	✓	7.3B	0.63	-	-	-	-	-	-	-	-	-
SD 3.0 [36]	×	8.0B	0.68	0.98	0.84	0.66	0.74	0.40	0.43	-	-	-
Emu3 [122]	✓	8.0B	0.54	0.98	0.71	0.34	0.81	0.17	0.21	-	-	-
Fluid [37]	✓	10.5B	0.69	0.96	0.83	0.63	0.80	0.39	0.51	-	-	-
FLUX.1.dev [60]	×	12.0B	-	-	-	-	-	-	-	0.7407	0.5718	0.6922
DALL-E 3 [12]	×	-	0.67	0.96	0.87	0.47	0.83	0.43	0.45	0.7785	0.6205	0.7036
Midjourney v6 [75]	×	-	0.63	0.96	0.81	0.56	0.83	0.22	0.42	0.7503	0.6885	0.6101

Table 3. Comprehensive comparison with state-of-the-art models on the GenEval [42] and T2I CompBench++ [53] benchmarks. All listed metrics are obtained without employing DPO and prompt rewriting techniques. The symbol ✓ denotes the use of the Next Token Prediction (NTP) strategy for image sampling. DALL-E 3 [12] and Midjourney v6 [75] are commercial closed-source models, and we do not have access to their exact model sizes.

fewer. While training with a random subset of tokens might limit the model’s ability to learn global features, we found that through dynamic resolution training, and leveraging the characteristics of VoPE, D-JEPA-T2I can quickly adapt to higher resolution generation.

Regarding the VAE encoding and decoding processes, when the image resolution surpasses 2K, we employ a tiling strategy, dividing the image into four parts for encoding/decoding to reduce memory consumption. Although this method may cause discontinuities at the edges, it is currently acceptable. Fig. 11 illustrates the results of image generation across a range from 1K to 4K, demonstrating the potential of D-JEPA-T2I for generating high-resolution images.

Inference Details. Empirically, we found that no more than 128 autoregressive steps are sufficient to generate images of any aspect ratio and resolution for D-JEPA-T2I. Therefore, unless otherwise specified, we use 128 autoregressive steps in our experiments. We observed that the classifier-free guidance (CFG) [48] significantly influences the quality of the generated images. A higher CFG often achieves better evaluation metrics on benchmarks like GenEval [42], but may compromise aesthetic qualities. Thus, in practice, for the experiments shown in Tab. 1 and Tab. 3, we set the CFG value to 6.0, while in other scenarios, we set it to 2.0. Additionally, we use a time shifting factor,

as described in [41], to adjust the allocation of steps in the denoising process. Through grid search, we determined this value to be 4.5.

10. Human Evaluation

We curated a comprehensive human evaluation benchmark by selecting 532 challenging and representative prompts from GenEval [42], T2I-CompBench [53], PickScore [59], and Parti-prompts [131]. This benchmark assesses the generated images based on their adherence to prompts, coherence, and realism.

To evaluate human preferences across these categories, raters were presented with paired outputs from two models and asked the following questions:

- *Prompt Adherence:* Which image more accurately represents and faithfully follows the provided text?
- *Coherence:* Which image better encapsulates the elements specified in the description?
- *Realism:* Given the prompt, which image exhibits higher quality and realism?

For each question, raters assessed the images as “better”, “same”, or “worse” when comparing outputs from different models. The questions were prioritized with prompt adherence being most critical, followed by coherence, and then realism. If a “same” result was reached at one priority level, only then were results at the subsequent level considered.

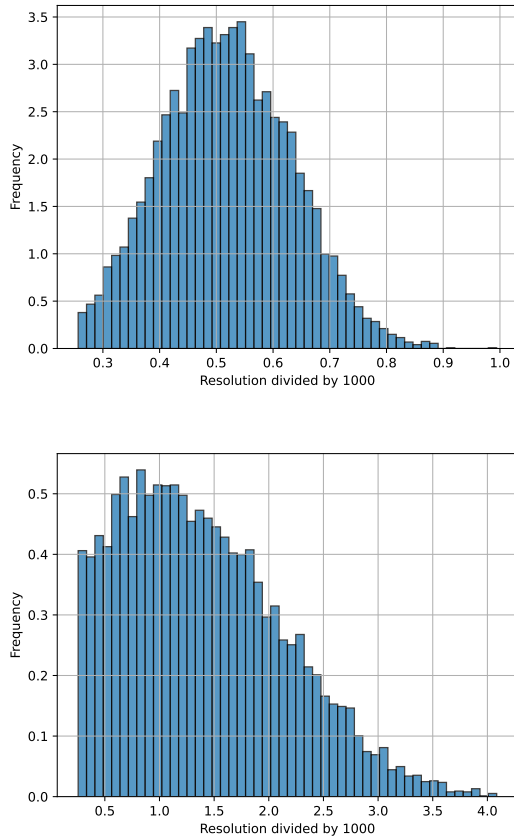


Figure 10. Dynamic resolution distribution during phase two training. Left: $\text{trunc_norm}(0.512, 0.12, 0.256, 1.024)$, primarily used to ensure the model can generate images with any aspect ratio and resolution within 1k resolution. Right: $\text{trunc_norm}(1.024, 1.0, 0.256, 4.096)$, used to extend the model’s capability to generate images from 1k to 4k resolution.

The win rate for each model against Midjourney v6 [75], as shown in Fig. 6, is calculated using the formula:

$$\text{win rate} = \frac{\#\text{better} + 0.5 \times \#\text{same}}{\#\text{better} + \#\text{same} + \#\text{worse}}$$

11. Ablation Study of Data Feedback

Statistical Analysis Sampling Accelerates Early-Stage Model Convergence. Data feedback plays a crucial role in improving the convergence speed of the model. By continuously analyzing the performance of generated images and adjusting the training dataset accordingly, the model learns more effectively from iterations that most significantly reduce errors and enhance accuracy. This targeted learning approach enables the model to converge faster than traditional static training methods. As shown in Tab. 4, by comparing experiments AB and CD, we achieve an overall score of 0.50 within 100k steps on the GenEval [42] bench-

mark using statistical analysis sampling. In contrast, with random sampling, even after 200k steps, the model only reaches a score of 0.48. This results in an almost twofold improvement in convergence speed.

Critic Model Sampling Effectively Mitigates Failure Cases in Late-Stage Training. By comparing experiments DE and FG, we find that critic model sampling with automated annotation further accelerates model convergence. With this approach, we achieve an overall score of 0.63 on GenEval at around 200k training steps. In contrast, relying solely on statistical analysis sampling requires 300k iterations to reach the same performance.

Our experiments (HI) further demonstrate that incorporating critic model sampling with human annotation substantially reduces failure cases (illustrated in Fig. 12) in the later stages of training. By dynamically adjusting the data distribution based on model performance, the critic model ensures a more balanced and robust learning process, leading to improved overall generation quality. Correspondingly, the model’s win rate against Midjourney v6 significantly increases from 17.3% to 35.6%, underscoring the crucial role of data feedback in enhancing model performance.

12. Properties of VoPE

Arbitrary Aspect Ratios and Continuous Resolutions Generation. Due to VoPE’s ability to consistently align all images to the reference grid size $g \times g$ during training, it ensures that images maintain consistency and plausibility in content when generating at any aspect ratio and continuous resolution, preventing distortions. This flexibility is vital for adapting the model to various use cases where specific image dimensions are needed. Fig. 13, 14, 15 and 16 show some samples generated by D-JEPA-T2I, demonstrating that regardless of extreme aspect ratios or resolutions, D-JEPA-T2I can produce coherent, high-quality images.

Layout Control by Relative Positional Offset b . During training, the pixel normalization operation involved in VoPE ensures that each image aligns to the center of the reference grid, achieved through the relative positional offset b . In the inference phase, we can manipulate the relative positional offset b to control the layout of the generated image, particularly when the generated objects are off-center or the main subject is incomplete. Fig. 17 illustrates how adjusting the relative positional offset b can alter the overall layout to produce more satisfactory results.

13. Visual Comparison with Other Methods

In this section, we present a visual comparison of the images generated by D-JEPA-T2I with those produced by



Figure 11. Ultra-high-resolution images generated by D-JEPA-T2I.

Group	Steps~(k)	SAS	CMS(Auto)	CMS(Human)	GenEval Overall	Win Rate(%)
A	0 ~ 100	w/o	w/o	w/o	0.38	-
B	100 ~ 200	w/o	w/o	w/o	0.48	-
C	0 ~ 100	w/	w/o	w/o	0.50	-
D	100 ~ 200	w/	w/o	w/o	0.60	-
E	200 ~ 300	w/	w/o	w/o	0.63	-
F	100 ~ 200	w/	w/	w/o	0.63	-
G	200 ~ 300	w/	w/	w/o	0.66	-
H	300 ~ 600	w/	w/	w/o	-	17.3
I	300 ~ 600	w/	w/o	w/	-	35.6

Table 4. Ablation study on data feedback. SAS: Statistical Analysis Sampling, CMS (Auto): Critic Model Sampling with automated annotation, CMS (Human): Critic Model Sampling with human annotation. The reported win rate is measured against Midjourney V6.

other state-of-the-art methods. This allows for a qualitative assessment of the capabilities and advantages of D-JEPA-T2I in generating high-quality images across various scenarios and styles. Through side-by-side comparisons, we can evaluate how well each method captures details, maintains image consistency, and handles different resolutions and aspect ratios.

In Fig. 18, 19, 20, 21, 22 and 23, the examples displayed highlight specific attributes of image quality, such as clarity, color accuracy, and complexity of details. These comparisons help demonstrate the strengths and potential limitations of different models in addressing diverse visual tasks.

14. Limitation

Limitations due to training data. In our training process, we excluded images containing text, which limits D-JEPA-T2I’s capability to perform text generation tasks. This may hinder its application in contexts where text is critical, such as in advertisements and posters. Moreover, D-JEPA-T2I currently only supports English prompts and cannot yet accommodate prompts in other languages like Chinese. Its performance is also less than optimal when generating high-resolution images (4k). However, these limitations can be addressed by integrating more diverse data types and improving data quality.

Limitations due to inference efficiency. While D-JEPA-T2I utilizes a next set-of-tokens prediction strategy for training and inference, it relies on bi-directional attention. This requirement precludes employing a key-value cache mechanism, which can speed up inference as seen with causal attention. Generating a 1k resolution image typically takes around a minute, imposing constraints on its use in highly interactive applications. Enhancements in inference efficiency could be achieved through feature compression techniques, as discussed in Chen et al. [22].

Limitations due to model size. Our current model is trained with 2.6B parameters, and we have not yet investigated performance at larger scales, such as over 10B parameters. Although the 2.6B model delivers satisfactory image generation, it still faces challenges in accurately generating specific entities and nouns, especially for people and places. Its performance is also lacking for prompts involving numerical, spatial relationships, and complex scenarios. Increasing the model size is expected to significantly improve its overall performance, as evidenced by findings in Esser et al. [36].

15. Prompts

All prompts are listed in the order of the corresponding images in the picture from top to bottom, from left to right.

The prompts used in Fig. 7.

- A young girl’s face disintegrates while beautiful colors fill her features, depicted in fluid dynamic brushwork with colorful dream-like illustrations.
- Close-up portrait of a young woman with long brown hair, neutral expression, soft lighting, minimalistic style, indoor setting, eye level.
- Stars, water, brilliantly, gorgeous large scale scene, a little girl, in the style of dreamy realism.
- Portrait of an elderly man with a white beard and a smile, close-up shot, realistic style, warm lighting, indoor setting, detailed.
- A smiling elderly man with gray hair and beard, wearing a black and white checkered shirt, close-up shot, neutral background, realistic style, eye level.
- Art collection style and fashion shoot, in the style of made of glass, dark blue and light pink, paul rand, solarpunk, camille vivier, beth didonato hair, barbiecore, hyper-realistic.
- A watercolor portrait of a Terrier dog, smiling and making a cute facial expression while looking at the camera, in Pixar style.



Figure 12. Common failure cases in image generation (without data feedback). Notably, training with data feedback can significantly reduce these failure cases.

- Nature vs. human nature, surreal, UHD, 8k, hyper details, rich colors, photograph.
- Graffiti of a funny dog on a street wall.
- Detailed pen and ink drawing of a massive complex alien space ship above a farm in the middle of nowhere.
- A close-up of a chibi-style figurine with a brown beard, blue eyes, and a green shirt with a yellow emblem, holding a gray stuffed animal, standing on a white surface with a blurred background, realistic style, warm lighting, detailed.
- A pair of old boots covered in mud.
- An entire universe inside a bottle sitting on the shelf at walmart on sale.
- Film still of a long-legged cute big-eye anthropomorphic cheeseburger wearing sneakers relaxing on the couch in a sparsely decorated living room.
- Human life depicted entirely out of fractals.
- Three trees with autumn leaves reflected in a calm lake, surrounded by fog, multiple entities, vibrant colors including yellow, orange, and red, balanced composition, realistic style, long shot.
- Grilled skewers of chicken and bell peppers, multiple entities, vibrant colors including yellow, red, and green, close-up, realistic style, outdoor setting, daylight.
- A panoramic view of a sunflower field with vibrant yellow and green hues, rolling hills in the background, a small village with red-roofed buildings, and a clear blue sky, captured in a realistic style with a wide shot perspective.
- Two small boats docked at a wooden pier on a calm lake, with a lush green forest in the background, warm lighting, realistic style, medium shot.
- Three spheres made of glass falling into ocean. Water is splashing. Sun is setting.
- A pristine white teapot with delicate blue floral designs, steaming with hot tea, sitting on a round wooden table.
- A chocolate cake with a dusting of powdered sugar, cut into eight slices, placed on a piece of parchment paper on a wooden surface, with a glass of honey and a fork on the side, realistic style, close-up, warm lighting.
- Stinky Tofu.
- Grilled skewers of chicken and bell peppers, multiple entities, vibrant colors including yellow, red, and green, close-up, realistic style, outdoor setting, daylight.

The prompts used in Fig. 12.

- A close-up of a metal staircase with a complex, interlocking design, featuring multiple levels and railings, in a monochromatic color scheme, with a focus on the geometric patterns and structural details, in a photorealistic style.
- A geometric metal structure with a series of intersecting lines and angles, creating a dynamic and abstract pattern, viewed from a low angle, minimalist style, black and



Figure 13. D-JEPA-T2I can generate arbitrary aspect ratios and continuous resolutions with VoPE. Prompt: “A gorgeous mountain landscape at sunset. Masterful painting by Rembrandt.”

- white photograph.
- A collection of fabric swatches in various colors and patterns, including shades of brown, green, gold, and gray, arranged in a grid pattern on a white background, with a focus on texture and detail, in a realistic style.
- A desert scene with a sand dune leading to a bright light source at the horizon, the Milky Way visible in the night

- sky, long exposure, minimalistic style, black and white.
- A white ceramic bowl with a textured pattern, placed on a woven bamboo mat, on a dark wooden table, minimalistic style, close-up.
- A white ceramic bowl with a textured pattern, placed on a woven bamboo mat, on a dark wooden table, minimalistic style, close-up.

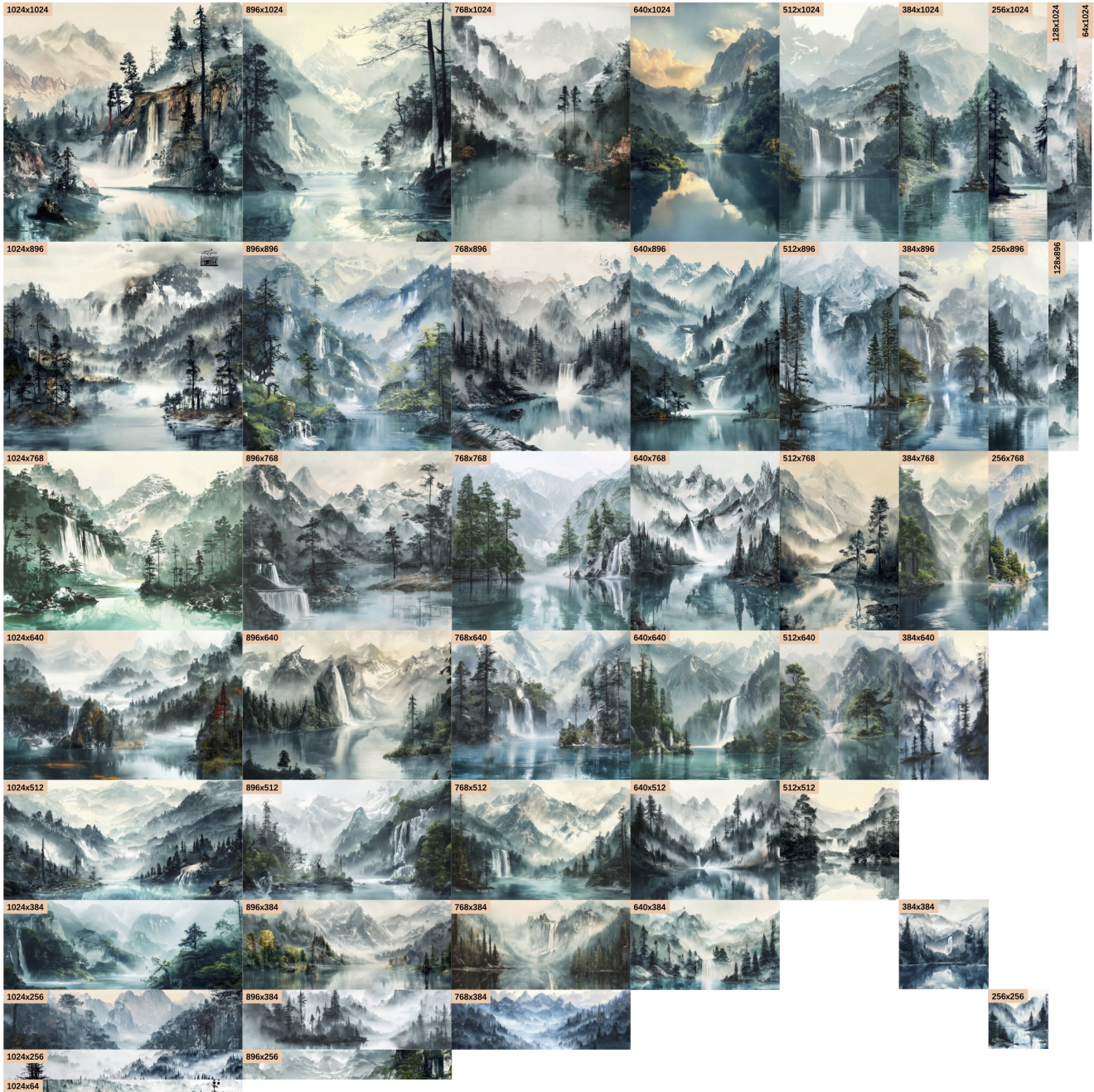


Figure 14. D-JEPA-T2I can generate arbitrary aspect ratios and continuous resolutions with VoPE. Prompt: “A serene mountain landscape in the style of a Chinese ink painting, with a waterfall cascading down into a crystal-clear lake surrounded by ancient pines.”

- A close-up of a single water droplet in mid-air, with a splash of water droplets surrounding it, against a white background, realistic style, high-definition.
- A geometric abstract composition featuring a mix of black and white polygons, with a focus on the spatial relationship between the shapes, minimalistic style, and a modern, clean aesthetic.

The prompts used in Fig. 11.

- A black and white photograph of a woman wearing a wide-brimmed hat, with a close-up shot of her face revealing delicate facial features, high contrast.
- Close-up of a brown horse with a white blaze on its face, standing in a misty field, realistic style, detailed, natural lighting, outdoor setting, long shot.



Figure 15. D-JEPA-T2I can generate arbitrary aspect ratios and continuous resolutions with VoPE. Prompt: “A still life of a vase overflowing with vibrant flowers, painted in bold colors and textured brushstrokes, reminiscent of van Gogh’s iconic style.”

- Single tree with vibrant yellow leaves standing in a calm lake, surrounded by mountains, reflected in the still water, autumnal colors, long shot, photorealistic style, natural lighting.

References

- [1] Josh Achiam, Steven Adler, Sandhini Agarwal, Lama Ahmad, Ilge Akkaya, Florencia Leoni Aleman, Diogo Almeida, Janko Altschmidt, Sam Altman, Shyamal Anadkat, et al. Gpt-4 technical report. *arXiv preprint arXiv:2303.08774*, 2023. 1, 3
- [2] Michael S. Albergo and Eric Vanden-Eijnden. Building

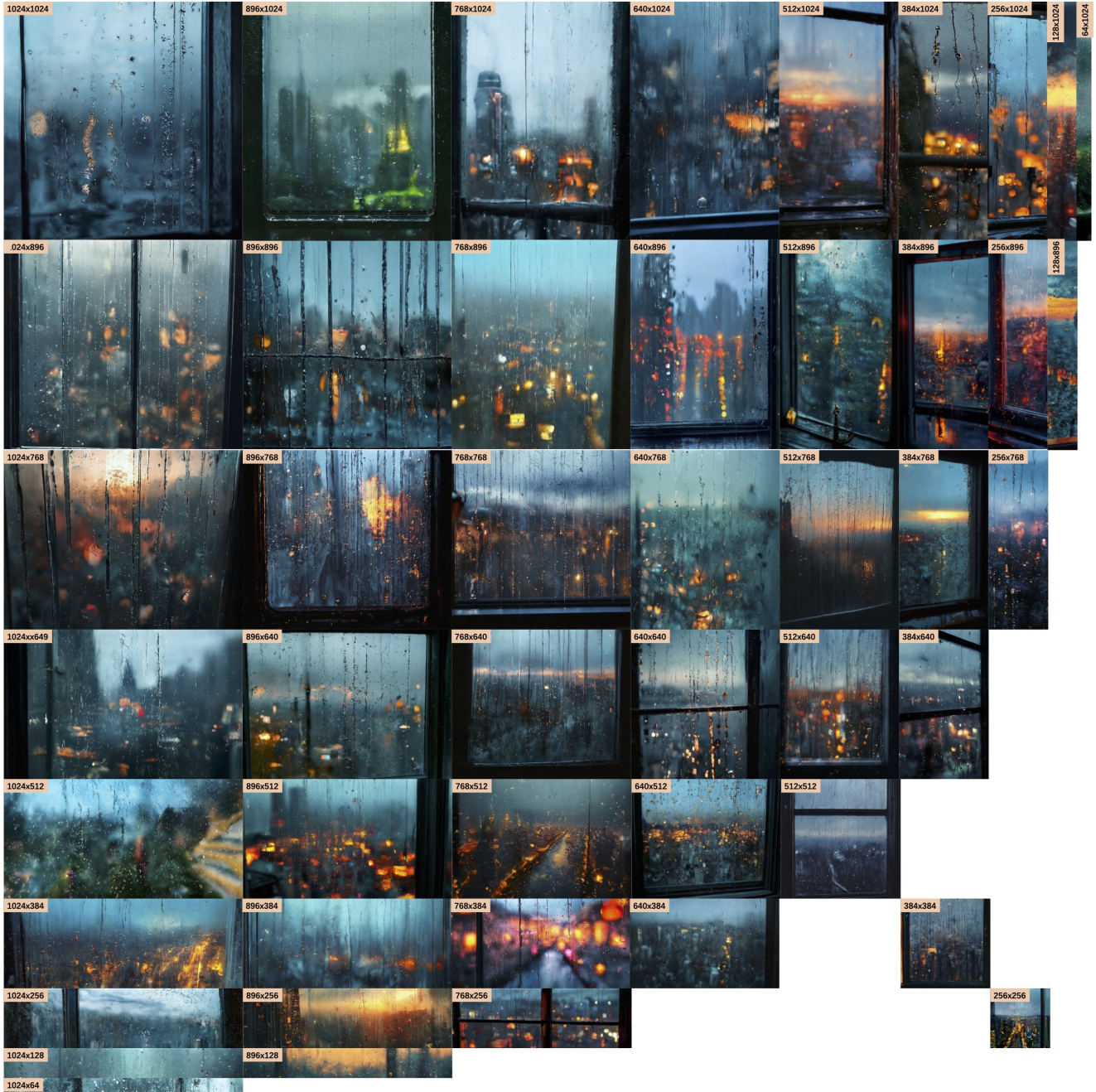


Figure 16. D-JEPA-T2I can generate arbitrary aspect ratios and continuous resolutions with VoPE. Prompt: “A window with raindrops trickling down, overlooking a blurry city.”

- normalizing flows with stochastic interpolants, 2022. 1
- [3] Michael S Albergo, Nicholas M Boffi, and Eric Vanden-Eijnden. Stochastic interpolants: A unifying framework for flows and diffusions. *arXiv preprint arXiv:2303.08797*, 2023. 3
- [4] Rohan Anil, Andrew M Dai, Orhan Firat, Melvin Johnson, Dmitry Lepikhin, Alexandre Passos, Siamak Shakeri, Emanuel Taropa, Paige Bailey, Zhifeng Chen, et al. Palm 2 technical report. *arXiv preprint arXiv:2305.10403*, 2023. 1
- [5] Jinze Bai, Shuai Bai, Yunfei Chu, Zeyu Cui, Kai Dang, Xiaodong Deng, Yang Fan, Wenbin Ge, Yu Han, Fei Huang, et al. Qwen technical report. *arXiv preprint arXiv:2309.16609*, 2023. 1
- [6] Yogesh Balaji, Seungjun Nah, Xun Huang, Arash Vahdat, Jiaming Song, Qinsheng Zhang, Karsten Kreis, Miika Aittala, Timo Aila, Samuli Laine, Bryan Catanzaro, Tero Kar-



Figure 17. Layout control by relative positional offset b . By adjusting b , we can generate more desirable layouts for selection.

- ras, and Ming-Yu Liu. ediff-i: Text-to-image diffusion models with an ensemble of expert denoisers, 2022. 1
- [7] Fan Bao, Chongxuan Li, Jun Zhu, and Bo Zhang. Analytic-dpm: an analytic estimate of the optimal reverse variance in diffusion probabilistic models. *arXiv preprint arXiv:2201.06503*, 2022. 1
- [8] Fan Bao, Shen Nie, Kaiwen Xue, Yue Cao, Chongxuan Li, Hang Su, and Jun Zhu. All are worth words: A vit backbone for diffusion models. In *Proceedings of the IEEE/CVF conference on computer vision and pattern recognition*, pages 22669–22679, 2023. 1
- [9] Fan Bao, Chendong Xiang, Gang Yue, Guande He, Hongzhou Zhu, Kaiwen Zheng, Min Zhao, Shilong Liu, Yaole Wang, and Jun Zhu. Vidu: a highly consistent, dynamic and skilled text-to-video generator with diffusion models. *arXiv preprint arXiv:2405.04233*, 2024. 1
- [10] Hangbo Bao, Li Dong, Songhao Piao, and Furu Wei. Beit: Bert pre-training of image transformers. *arXiv preprint arXiv:2106.08254*, 2021. 1
- [11] Omer Bar-Tal, Hila Chefer, Omer Tov, Charles Herrmann, Roni Paiss, Shiran Zada, Ariel Ephrat, Junhwa Hur, Yuanzhen Li, Tomer Michaeli, et al. Lumiere: A space-time diffusion model for video generation. *arXiv preprint arXiv:2401.12945*, 2024. 1
- [12] James Betker, Gabriel Goh, Li Jing, Tim Brooks, Jianfeng Wang, Linjie Li, Long Ouyang, Juntang Zhuang, Joyce Lee, Yufei Guo, et al. Improving image generation with better captions. *Computer Science*. <https://cdn.openai.com/papers/dall-e-3.pdf>, 2(3), 2023. 1, 7, 8, 4, 14
- [13] Andreas Blattmann, Tim Dockhorn, Sumith Kulal, Daniel Mendelevitch, Maciej Kilian, Dominik Lorenz, Yam Levi, Zion English, Vikram Voleti, Adam Letts, et al. Stable video diffusion: Scaling latent video diffusion models to large datasets. *arXiv preprint arXiv:2311.15127*, 2023.
- [14] Andreas Blattmann, Robin Rombach, Huan Ling, Tim Dockhorn, Seung Wook Kim, Sanja Fidler, and Karsten Kreis. Align your latents: High-resolution video synthesis with latent diffusion models. In *Proceedings of the IEEE/CVF Conference on Computer Vision and Pattern Recognition*, pages 22563–22575, 2023. 1
- [15] T. Brooks, B. Peebles, C. Holmes, W. DePue, Y. Guo, L. Jing, D. Schnurr, J. Taylor, T. Luhman, E. Luhman, C. Ng, R. Wang, and A. Ramesh. Video generation models as world simulators. *OpenAI*, 2024. 1
- [16] Tom B Brown. Language models are few-shot learners. *arXiv preprint arXiv:2005.14165*, 2020. 1
- [17] Huiwen Chang, Han Zhang, Lu Jiang, Ce Liu, and William T Freeman. Maskgit: Masked generative image transformer. In *Proceedings of the IEEE/CVF Conference on Computer Vision and Pattern Recognition*, pages 11315–11325, 2022. 4, 1
- [18] Huiwen Chang, Han Zhang, Jarred Barber, AJ Maschinot, Jose Lezama, Lu Jiang, Ming-Hsuan Yang, Kevin Murphy, William T Freeman, Michael Rubinstein, et al. Muse: Text-to-image generation via masked generative transformers. *arXiv preprint arXiv:2301.00704*, 2023. 1
- [19] Dehao Chen, Chiachen Chou, Yuanzhong Xu, and Jonathan Hseu. Bfloat16: The secret to high performance on cloud tpus, 2019. 2
- [20] Dengsheng Chen, Jie Hu, Xiaoming Wei, and Enhua Wu. Denoising with a joint-embedding predictive architecture. *arXiv preprint arXiv:2410.03755*, 2024. 1, 2, 3, 5, 7
- [21] Junsong Chen, Jincheng Yu, Chongjian Ge, Lewei Yao, Enze Xie, Yue Wu, Zhongdao Wang, James Kwok, Ping Luo, Huchuan Lu, et al. Pixart- α : Fast training of diffusion transformer for photorealistic text-to-image synthesis. *arXiv preprint arXiv:2310.00426*, 2023. 7, 8, 1, 4, 17
- [22] Junsong Chen, Chongjian Ge, Enze Xie, Yue Wu, Lewei Yao, Xiaozhe Ren, Zhongdao Wang, Ping Luo, Huchuan Lu, and Zhenguo Li. Pixart- σ : Weak-to-strong training of diffusion transformer for 4k text-to-image generation. *arXiv preprint arXiv:2403.04692*, 2024. 1, 7
- [23] Ricky TQ Chen, Yulia Rubanova, Jesse Bettencourt, and David K Duvenaud. Neural ordinary differential equations. *Advances in neural information processing systems*, 31, 2018. 1
- [24] Zhe Chen, Jiannan Wu, Wenhai Wang, Weijie Su, Guo Chen, Sen Xing, Muyan Zhong, Qinglong Zhang, Xizhou Zhu, Lewei Lu, Bin Li, Ping Luo, Tong Lu, Yu Qiao, and Jifeng Dai. Internvl: Scaling up vision foundation models and aligning for generic visual-linguistic tasks. *arXiv preprint arXiv:2312.14238*, 2023. 7, 3
- [25] Zhe Chen, Weiyun Wang, Hao Tian, Shenglong Ye, Zhangwei Gao, Erfei Cui, Wenwen Tong, Kongzhi Hu, Jiapeng Luo, Zheng Ma, et al. How far are we to gpt-4v? closing the gap to commercial multimodal models with open-source suites. *arXiv preprint arXiv:2404.16821*, 2024. 7

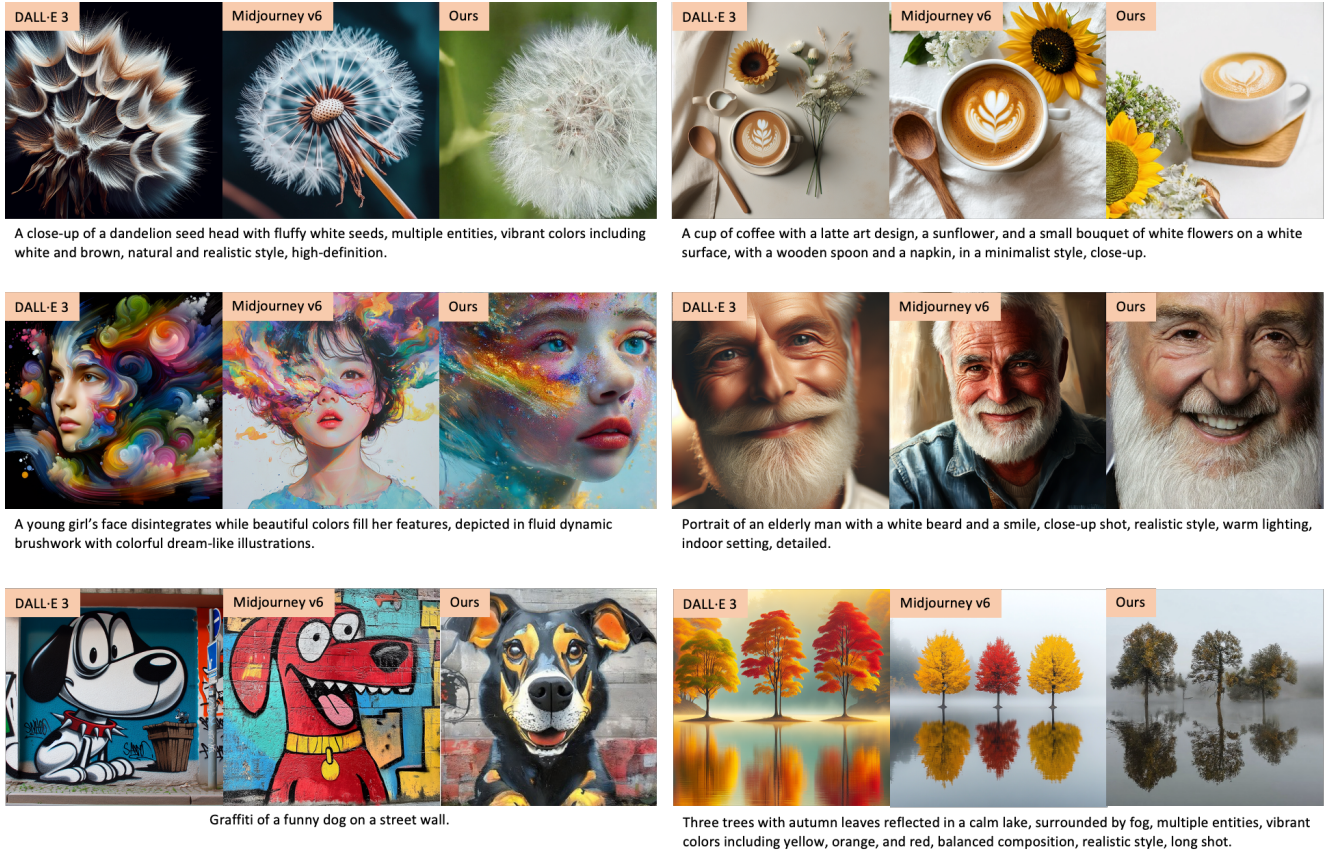


Figure 18. Visual comparison among commercial models, *i.e.*, DALL-E 3 [12], Midjourney v6 [75], and D-JEPA-T2I.

[26] Aakanksha Chowdhery, Sharan Narang, Jacob Devlin, Maarten Bosma, Gaurav Mishra, Adam Roberts, Paul Barham, Hyung Won Chung, Charles Sutton, Sebastian Gehrmann, et al. Palm: Scaling language modeling with pathways. *Journal of Machine Learning Research*, 24(240): 1–113, 2023. 1

[27] Hyung Won Chung, Le Hou, Shayne Longpre, Barret Zoph, Yi Tay, William Fedus, Yunxuan Li, Xuezhi Wang, Mostafa Dehghani, Siddhartha Brahma, et al. Scaling instruction-finetuned language models. *Journal of Machine Learning Research*, 25(70):1–53, 2024. 3

[28] Xiaoliang Dai, Ji Hou, Chih-Yao Ma, Sam Tsai, Jialiang Wang, Rui Wang, Peizhao Zhang, Simon Vandenhende, Xiaofang Wang, Abhimanyu Dubey, Matthew Yu, Abhishek Kadian, Filip Radenovic, Dhruv Mahajan, Kungpeng Li, Yue Zhao, Vladan Petrovic, Mitesh Kumar Singh, Simran Motwani, Yi Wen, Yiwen Song, Roshan Sumbaly, Vignesh Ramanathan, Zijian He, Peter Vajda, and Devi Parikh. Emu: Enhancing image generation models using photogenic needles in a haystack, 2023. 1

[29] Quan Dao, Hao Phung, Binh Nguyen, and Anh Tran. Flow matching in latent space, 2023. 1

[30] Mostafa Dehghani, Josip Djolonga, Basil Mustafa, Piotr Padlewski, Jonathan Heek, Justin Gilmer, Andreas Steiner, Mathilde Caron, Robert Geirhos, Ibrahim Al-abdulmohsin, Rodolphe Jenatton, Lucas Beyer, Michael Tschannen, Anurag Arnab, Xiao Wang, Carlos Riquelme, Matthias Minderer, Joan Puigcerver, Utku Evci, Manoj Kumar, Sjoerd van Steenkiste, Gamaleldin F. Elsayed, Aravindh Mahendran, Fisher Yu, Avital Oliver, Fantine Huot, Jasmijn Bastings, Mark Patrick Collier, Alexey Gritsenko, Vignesh Birodkar, Cristina Vasconcelos, Yi Tay, Thomas Mensink, Alexander Kolesnikov, Filip Pavetić, Dustin Tran, Thomas Kipf, Mario Lučić, Xiaohua Zhai, Daniel Keysers, Jeremiah Harmsen, and Neil Houlsby. Scaling vision transformers to 22 billion parameters, 2023. 2

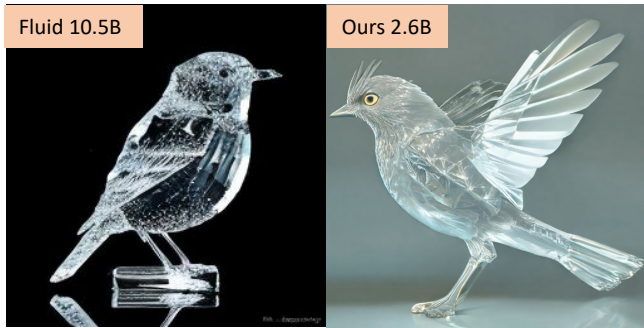
[31] Prafulla Dhariwal and Alexander Nichol. Diffusion models beat gans on image synthesis. In *Advances in neural information processing systems*, pages 8780–8794, 2021. 1

[32] Tim Dockhorn, Arash Vahdat, and Karsten Kreis. Score-based generative modeling with critically-damped langevin diffusion. *arXiv preprint arXiv:2112.07068*, 2021. 1

[33] Tim Dockhorn, Arash Vahdat, and Karsten Kreis. Genie: Higher-order denoising diffusion solvers, 2022. 1

[34] Alexey Dosovitskiy. An image is worth 16x16 words: Transformers for image recognition at scale. *arXiv preprint arXiv:2010.11929*, 2020. 2

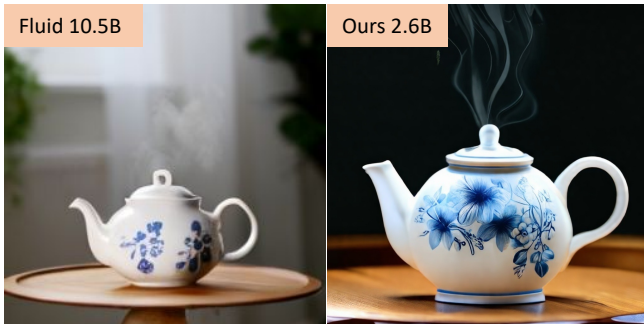
[35] Patrick Esser, Johnathan Chiu, Parmida Atighehchian, Jonathan Granskog, and Anastasis Germanidis. Structure and content-guided video synthesis with diffusion models.



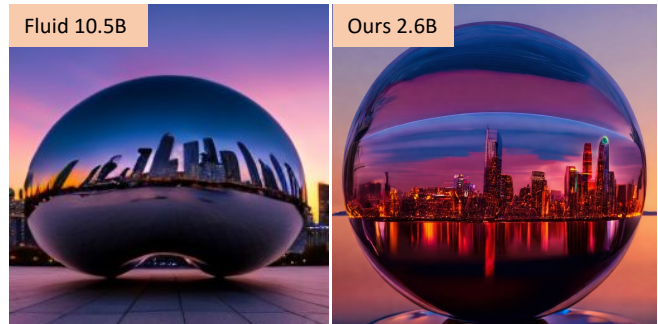
A bird made of crystal.



A white horse reading a book, fairytale.



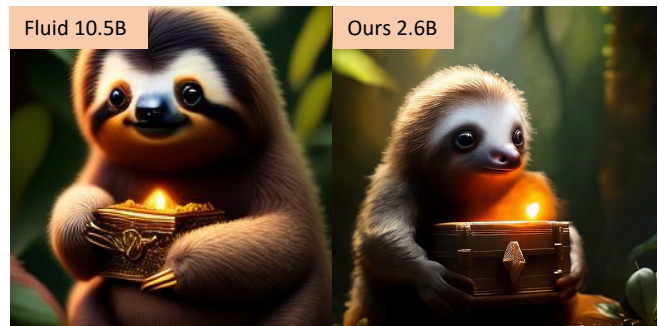
A pristine white teapot with delicate blue floral designs, steaming with hot tea, sitting on a round wooden table.



An image of a chrome sphere reflecting a vibrant city skyline at sunset.



Hot air balloons and flowers, collage art, photorealism, muted colors, 3D shading beautiful eldritch, mixed media, vaporous.



A close-up photo of a baby sloth holding a treasure chest. A warm, golden light emanates from within the chest, casting a soft glow on the sloth's fur and the surrounding rainforest foliage.

Figure 19. Visual comparison between Fluid [37] and D-JEPA-T2I.

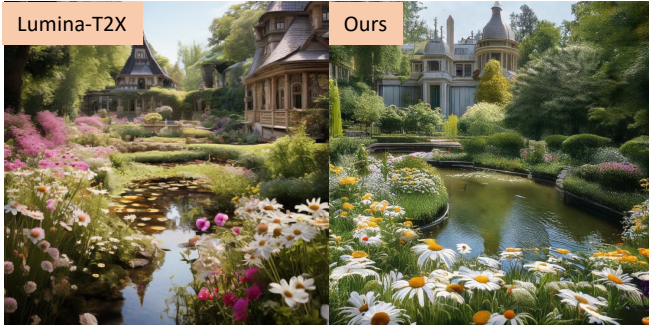
In *Proceedings of the IEEE/CVF International Conference on Computer Vision*, pages 7346–7356, 2023. 1

- [36] Patrick Esser, Sumith Kulal, Andreas Blattmann, Rahim Entezari, Jonas Müller, Harry Saini, Yam Levi, Dominik Lorenz, Axel Sauer, Frederic Boesel, et al. Scaling rectified flow transformers for high-resolution image synthesis. In *Forty-first International Conference on Machine Learning*, 2024. 1, 2, 3, 5, 7, 8, 4

- [37] Lijie Fan, Tianhong Li, Siyang Qin, Yuanzhen Li, Chen Sun, Michael Rubinstein, Deqing Sun, Kaiming He, and

Yonglong Tian. Fluid: Scaling autoregressive text-to-image generative models with continuous tokens. *arXiv preprint arXiv:2410.13863*, 2024. 8, 4, 15

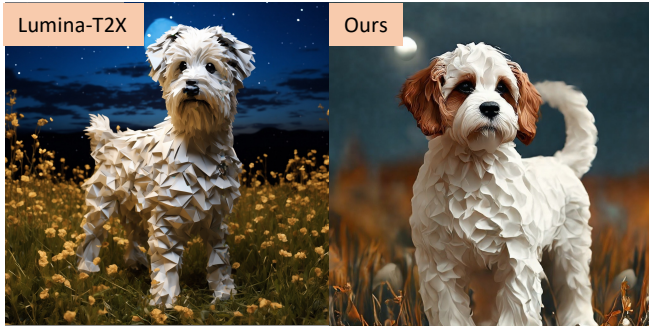
- [38] Zhida Feng, Zhenyu Zhang, Xintong Yu, Yewei Fang, Lanxin Li, Xuyi Chen, Yuxiang Lu, Jiaxiang Liu, Weichong Yin, Shikun Feng, et al. Ernie-vilg 2.0: Improving text-to-image diffusion model with knowledge-enhanced mixture-of-denoising-experts. In *Proceedings of the IEEE/CVF Conference on Computer Vision and Pattern Recognition*, pages 10135–10145, 2023. 7



A beautiful Victorian-era botanical garden featuring a charming pond and lovely daisies.



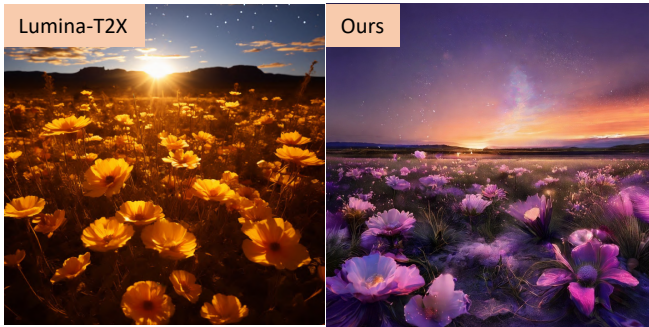
An impressionist painting of a bustling café terrace at night, with vivid colors and lively brush strokes.



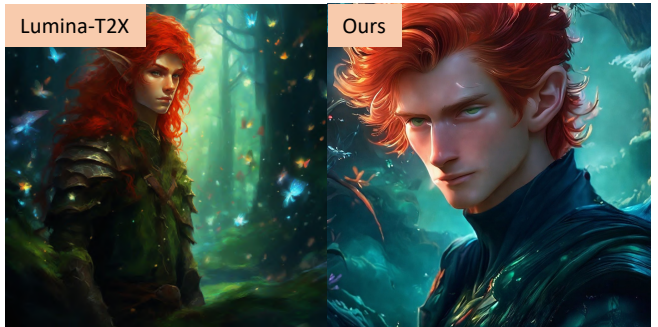
A photorealistic render of an origami white and tan mini Bernadoodle dog standing in a surrealistic field under the moonlit setting.



An old shaman woman adorned with feathers and leather, portrayed in a photorealistic illustration with soft lighting and sharp focus.



A photograph showcases the beauty of desert flowers and mirrors illuminated by the soft morning light. The image, extremely photorealistic and meticulously detailed, depicts a lonely desert atmosphere with stars shining overhead.



A red-haired male elf hunter with a shy expression is standing in a mystical forest, surrounded by fairy tale-like elements and vibrant spectral colors.

Figure 20. Visual comparison between Lumina-T2X [41] and D-JEPA-T2I.

[39] Johannes S Fischer, Ming Gui, Pingchuan Ma, Nick Stracke, Stefan A Baumann, and Björn Ommer. Boosting latent diffusion with flow matching. *arXiv preprint arXiv:2312.07360*, 2023. 1

[40] Deep Floyd. If: A github repository. <https://github.com/deep-floyd/IF>, 2023. 7

[41] Peng Gao, Le Zhuo, Ziyi Lin, Chris Liu, Junsong Chen, Ruoyi Du, Enze Xie, Xu Luo, Longtian Qiu, Yuhang Zhang, et al. Lumina-t2x: Transforming text into any modality, resolution, and duration via flow-based large diffusion transformers. *arXiv preprint arXiv:2405.05945*,

2024. 1, 3, 4, 7, 16

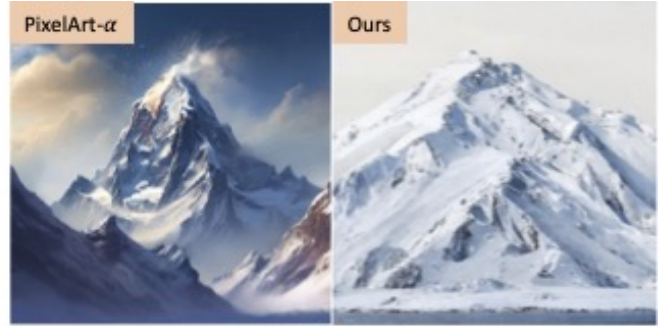
[42] Dhruva Ghosh, Hannaneh Hajishirzi, and Ludwig Schmidt. Geneval: An object-focused framework for evaluating text-to-image alignment. *Advances in Neural Information Processing Systems*, 36, 2024. 2, 7, 8, 3, 4, 5

[43] Agrim Gupta, Lijun Yu, Kihyuk Sohn, Xiuye Gu, Meera Hahn, Li Fei-Fei, Irfan Essa, Lu Jiang, and José Lezama. Photorealistic video generation with diffusion models, 2023. 1

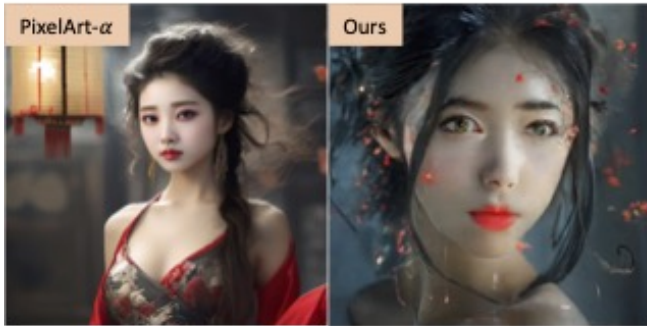
[44] Kaiming He, Xiangyu Zhang, Shaoqing Ren, and Jian Sun. Deep residual learning for image recognition. In *Proceed-*



Crocodile in a sweater.



A snowy mountain.



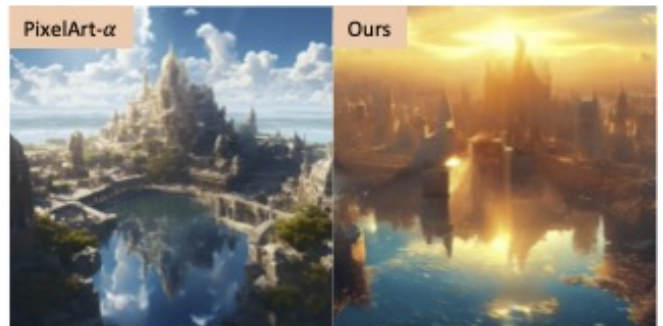
Real beautiful woman, Chinese.



A fisheye lens view of a turtle sitting in a forest.



A painting depicting a red wave outside, trapped emotions depicted, full body, Jon Foster, depth, Dima Dmitriev, fisheye effects, Ray Collins.



Bright scene, aerial view, ancient city, fantasy, gorgeous light, mirror reflection, high detail, wide angle lens.

Figure 21. Visual comparison between PixelArt- α [21] and D-JEPA-T2I.

ings of the *IEEE conference on computer vision and pattern recognition*, pages 770–778, 2016. 6

- [45] Kaiming He, Xinlei Chen, Saining Xie, Yanghao Li, Piotr Dollár, and Ross Girshick. Masked autoencoders are scalable vision learners. In *Proceedings of the IEEE/CVF conference on computer vision and pattern recognition*, pages 16000–16009, 2022. 1
- [46] Shuai He, Yongchang Zhang, Rui Xie, Dongxiang Jiang, and Anlong Ming. Rethinking image aesthetics assessment: Models, datasets and benchmarks. In *IJCAI*, pages 942–

948, 2022. 1

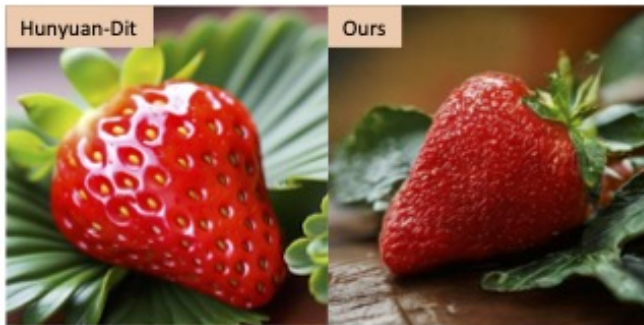
- [47] Jonathan Ho and Tim Salimans. Classifier-free diffusion guidance. In *NeurIPS 2021 Workshop on Deep Generative Models and Downstream Applications*, 2021. 8, 1
- [48] Jonathan Ho and Tim Salimans. Classifier-free diffusion guidance. *arXiv preprint arXiv:2207.12598*, 2022. 4
- [49] Jonathan Ho, Ajay Jain, and Pieter Abbeel. Denoising diffusion probabilistic models. In *Advances in neural information processing systems*, pages 6840–6851, 2020. 1
- [50] Jonathan Ho, William Chan, Chitwan Saharia, Jay Whang,



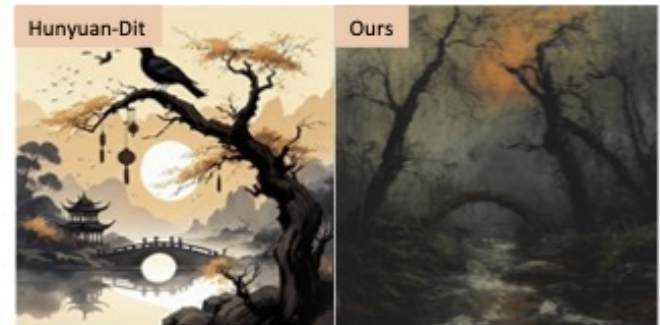
A clever fox walks in a broadleaf forest, next to a stream, details true, photography.



Stinky Tofu.



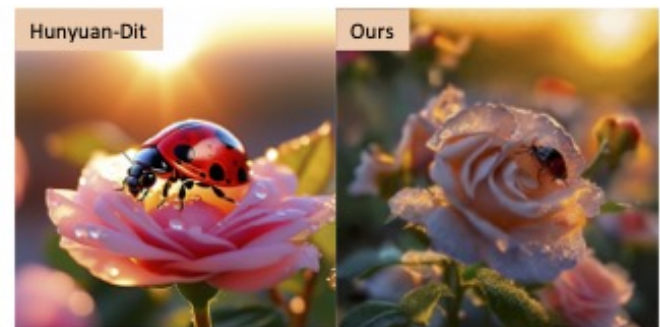
A close-up of a fresh strawberry, glorious, attempting color, lying on pale green leaves with brown table in the background.



Withered vines, old trees, there are some crows at dusk; A small bridge, flowing water, some huts.



The picture mainly depicts a Baroque vase with a gold decorative frame, the vase is blooming with various colorful flowers, white background.



The sun rises slightly, the dew on the rose petals in the garden is crystal clear, a ladybug is crawling to the dew, the background is the early morning garden, macro lens.

Figure 22. Visual comparison between HunyuanDit [65] and D-JEPA-T2I.

Ruiqi Gao, Alexey Gritsenko, Diederik P. Kingma, Ben Poole, Mohammad Norouzi, David J. Fleet, and Tim Salimans. Imagen video: High definition video generation with diffusion models, 2022. 1

[51] Jonathan Ho, Chitwan Saharia, William Chan, David J Fleet, Mohammad Norouzi, and Tim Salimans. Cascaded diffusion models for high fidelity image generation. *Journal of Machine Learning Research*, 23(47):1–33, 2022. 1

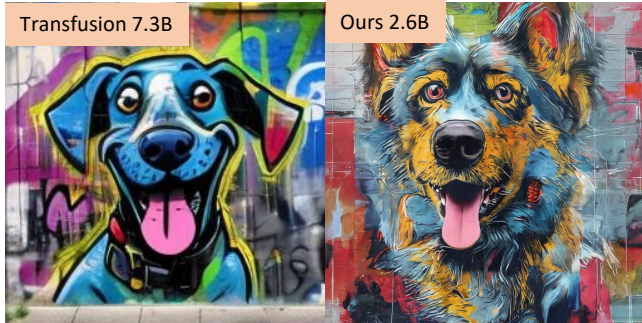
[52] Jordan Hoffmann, Sebastian Borgeaud, Arthur Mensch, Elena Buchatskaya, Trevor Cai, Eliza Rutherford, Diego de Las Casas, Lisa Anne Hendricks, Johannes Welbl, Aidan

Clark, et al. Training compute-optimal large language models. *arXiv preprint arXiv:2203.15556*, 2022. 1

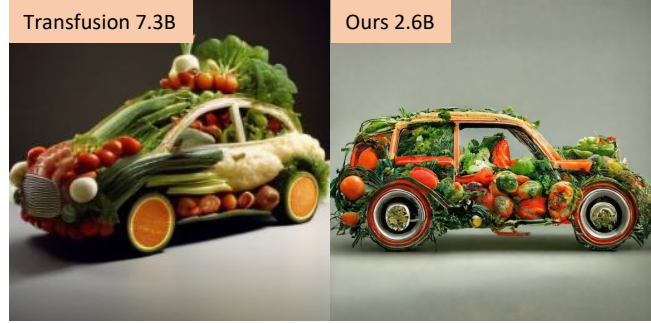
[53] Kaiyi Huang, Kaiyue Sun, Enze Xie, Zhenguo Li, and Xihui Liu. T2i-compbench: A comprehensive benchmark for open-world compositional text-to-image generation. *Advances in Neural Information Processing Systems*, 36:78723–78747, 2023. 2, 6, 8, 4

[54] Aapo Hyvärinen and Peter Dayan. Estimation of non-normalized statistical models by score matching. *Journal of Machine Learning Research*, 6(4), 2005. 1

[55] Tero Karras, Miika Aittala, Timo Aila, and Samuli Laine.



Graffiti of a funny dog on a street wall.



A car made out of vegetables.



A photo of a person with the head of a cow, wearing a tuxedo and black bowtie. Beach wallpaper in the background.

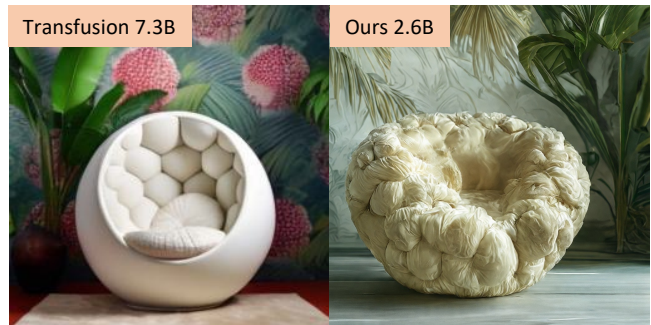
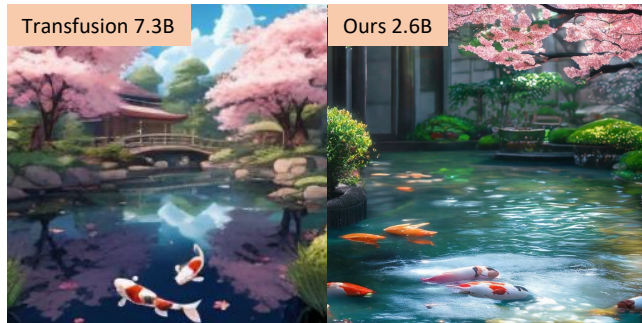


Photo of a lychee-inspired spherical chair, with a bumpy white exterior and plush interior, set against a tropical wallpaper.



A tranquil, anime-style koi pond in a serene Japanese garden, featuring blossoming cherry trees.



A raccoon wearing cowboy hat and black leather jacket is behind the backyard window. Rain droplets on the window.

Figure 23. Visual comparison between Transfusion [136] and D-JEPA-T2I.

Elucidating the design space of diffusion-based generative models. In *Advances in neural information processing systems*, pages 26565–26577, 2022. 1

[56] Jacob Devlin Ming-Wei Chang Kenton and Lee Kristina Toutanova. Bert: Pre-training of deep bidirectional transformers for language understanding. In *Proceedings of naacL-HLT*, page 2. Minneapolis, Minnesota, 2019. 1

[57] Maciej Kilian, Varun Jampani, and Luke Zettlemoyer. Computational tradeoffs in image synthesis: Diffusion, masked-token, and next-token prediction. *arXiv preprint arXiv:2405.13218*, 2024. 1

[58] Diederik Kingma and Ruiqi Gao. Understanding diffusion objectives as the elbo with simple data augmentation. *Advances in Neural Information Processing Systems*, 36, 2024. 1

[59] Yuval Kirstain, Adam Polyak, Uriel Singer, Shahbuland Matiana, Joe Penna, and Omer Levy. Pick-a-pic: An open dataset of user preferences for text-to-image generation. *Advances in Neural Information Processing Systems*, 36: 36652–36663, 2023. 8, 4

[60] Black Forest Labs. Flux.1: An open-source image generation model. <https://www.basedlabs.ai/tools/>

- [flux1](#), 2024. 4
- [61] Teven Le Scao, Angela Fan, Christopher Akiki, Ellie Pavlick, Suzana Ilić, Daniel Hesslow, Roman Castagné, Alexandra Sasha Luccioni, François Yvon, Matthias Gallé, et al. Bloom: A 176b-parameter open-access multilingual language model. 2023. 1
- [62] Sangyun Lee, Beomsu Kim, and Jong Chul Ye. Minimizing trajectory curvature of ode-based generative models, 2023. 1
- [63] Baiqi Li, Zhiqiu Lin, Deepak Pathak, Jiayao Li, Yixin Fei, Kewen Wu, Tiffany Ling, Xide Xia, Pengchuan Zhang, Graham Neubig, et al. Genai-bench: Evaluating and improving compositional text-to-visual generation. *arXiv preprint arXiv:2406.13743*, 2024. 2, 7, 8
- [64] Tianhong Li, Yonglong Tian, He Li, Mingyang Deng, and Kaiming He. Autoregressive image generation without vector quantization. *arXiv preprint arXiv:2406.11838*, 2024. 1, 3, 4
- [65] Zhimin Li, Jianwei Zhang, Qin Lin, Jiangfeng Xiong, Yanxin Long, Xinchu Deng, Yingfang Zhang, Xingchao Liu, Minbin Huang, Zedong Xiao, et al. Hunyuan-dit: A powerful multi-resolution diffusion transformer with fine-grained chinese understanding. *arXiv preprint arXiv:2405.08748*, 2024. 1, 5, 4, 18
- [66] Youwei Liang, Junfeng He, Gang Li, Peizhao Li, Arseniy Klimovskiy, Nicholas Carolan, Jiao Sun, Jordi Pont-Tuset, Sarah Young, Feng Yang, et al. Rich human feedback for text-to-image generation. In *Proceedings of the IEEE/CVF Conference on Computer Vision and Pattern Recognition*, pages 19401–19411, 2024. 2, 6
- [67] Yaron Lipman, Ricky TQ Chen, Heli Ben-Hamu, Maximilian Nickel, and Matt Le. Flow matching for generative modeling. *arXiv preprint arXiv:2210.02747*, 2022. 1, 3
- [68] Yaron Lipman, Ricky T. Q. Chen, Heli Ben-Hamu, Maximilian Nickel, and Matthew Le. Flow matching for generative modeling. In *The Eleventh International Conference on Learning Representations*, 2023. 1
- [69] Dongyang Liu, Shitian Zhao, Le Zhuo, Weifeng Lin, Yu Qiao, Hongsheng Li, and Peng Gao. Lumina-mgpt: Illuminate flexible photorealistic text-to-image generation with multimodal generative pretraining. *arXiv preprint arXiv:2408.02657*, 2024. 1
- [70] Xingchao Liu, Chengyue Gong, and Qiang Liu. Flow straight and fast: Learning to generate and transfer data with rectified flow. *arXiv preprint arXiv:2209.03003*, 2022. 1
- [71] Xingchao Liu, Xiwen Zhang, Jianzhu Ma, Jian Peng, and Qiang Liu. InstafLOW: One step is enough for high-quality diffusion-based text-to-image generation, 2023. 1
- [72] Ilya Loshchilov, Frank Hutter, et al. Fixing weight decay regularization in adam. *arXiv preprint arXiv:1711.05101*, 5, 2017. 2
- [73] Cheng Lu, Yuhao Zhou, Fan Bao, Jianfei Chen, Chongxuan Li, and Jun Zhu. Dpm-solver++: Fast solver for guided sampling of diffusion probabilistic models, 2023. 1
- [74] Nanye Ma, Mark Goldstein, Michael S. Albergo, Nicholas M. Boffi, Eric Vanden-Eijnden, and Saining Xie. Sit: Exploring flow and diffusion-based generative models with scalable interpolant transformers, 2024. 3, 1
- [75] Midjourney Community. Midjourney v6 - ai art generator, 2024. 7, 8, 4, 5, 14
- [76] Sicheng Mo, Fangzhou Mu, Kuan Heng Lin, Yanli Liu, Bochen Guan, Yin Li, and Bolei Zhou. Freecontrol: Training-free spatial control of any text-to-image diffusion model with any condition. In *Proceedings of the IEEE/CVF Conference on Computer Vision and Pattern Recognition*, pages 7465–7475, 2024. 3
- [77] Alex Nichol, Prafulla Dhariwal, Aditya Ramesh, Pranav Shyam, Pamela Mishkin, Bob McGrew, Ilya Sutskever, and Mark Chen. Glide: Towards photorealistic image generation and editing with text-guided diffusion models. *arXiv preprint arXiv:2112.10741*, 2021. 1
- [78] Long Ouyang, Jeffrey Wu, Xu Jiang, Diogo Almeida, Carroll Wainwright, Pamela Mishkin, Chong Zhang, Sandhini Agarwal, Katarina Slama, Alex Ray, et al. Training language models to follow instructions with human feedback. *Advances in neural information processing systems*, 35: 27730–27744, 2022. 1
- [79] I. Pavlov, A. Ivanov, and S. Stafievskiy. Text-to-Image Benchmark: A benchmark for generative models. <https://github.com/boomb0om/text2image-benchmark>, 2023. Version 0.1.0. 3
- [80] William Peebles and Saining Xie. Scalable diffusion models with transformers. In *Proceedings of the IEEE/CVF International Conference on Computer Vision*, pages 4195–4205, 2023. 2, 5, 1
- [81] Bowen Peng and Jeffrey Quesnelle. Ntk-aware scaled rope allows llama models to have extended (8k+) context size without any fine-tuning and minimal perplexity degradation, 2023. 4
- [82] Ethan Perez, Florian Strub, Harm De Vries, Vincent Dumoulin, and Aaron Courville. Film: Visual reasoning with a general conditioning layer. In *Proceedings of the AAAI conference on artificial intelligence*, 2018. 2
- [83] Dustin Podell, Zion English, Kyle Lacey, Andreas Blattmann, Tim Dockhorn, Jonas Müller, Joe Penna, and Robin Rombach. Sdxl: Improving latent diffusion models for high-resolution image synthesis, 2023. 1, 7, 8, 4
- [84] Aram-Alexandre Pooladian, Heli Ben-Hamu, Carles Domingo-Enrich, Brandon Amos, Yaron Lipman, and Ricky T. Q. Chen. Multisample flow matching: Straightening flows with minibatch couplings, 2023. 1
- [85] Alec Radford. Improving language understanding by generative pre-training. 2018. 1
- [86] Alec Radford, Jeffrey Wu, Rewon Child, David Luan, Dario Amodei, Ilya Sutskever, et al. Language models are unsupervised multitask learners. *OpenAI blog*, 1(8):9, 2019. 1
- [87] Rafael Rafailov, Archit Sharma, Eric Mitchell, Christopher D Manning, Stefano Ermon, and Chelsea Finn. Direct preference optimization: Your language model is secretly a reward model. *Advances in Neural Information Processing Systems*, 36, 2024. 2, 6
- [88] Colin Raffel, Noam Shazeer, Adam Roberts, Katherine Lee, Sharan Narang, Michael Matena, Yanqi Zhou, Wei Li,

- and Peter J Liu. Exploring the limits of transfer learning with a unified text-to-text transformer. *Journal of machine learning research*, 21(140):1–67, 2020. 1
- [89] Aditya Ramesh, Mikhail Pavlov, Gabriel Goh, Scott Gray, Chelsea Voss, Alec Radford, Mark Chen, and Ilya Sutskever. Zero-shot text-to-image generation. In *International conference on machine learning*, pages 8821–8831. Pmlr, 2021. 1
- [90] Aditya Ramesh, Prafulla Dhariwal, Alex Nichol, Casey Chu, and Mark Chen. Hierarchical text-conditional image generation with clip latents, 2022. 1, 4
- [91] Jeff Rasley, Samyam Rajbhandari, Olatunji Ruwase, and Yuxiong He. Deepspeed: System optimizations enable training deep learning models with over 100 billion parameters. In *Proceedings of the 26th ACM SIGKDD International Conference on Knowledge Discovery & Data Mining*, pages 3505–3506, 2020. 3
- [92] Ali Razavi, Aaron Van den Oord, and Oriol Vinyals. Generating diverse high-fidelity images with vq-vae-2. *Advances in neural information processing systems*, 32, 2019. 1
- [93] Robin Rombach, Andreas Blattmann, Dominik Lorenz, Patrick Esser, and Björn Ommer. High-resolution image synthesis with latent diffusion models. In *Proceedings of the IEEE/CVF conference on computer vision and pattern recognition*, pages 10684–10695, 2022. 1, 7, 4
- [94] Olga Russakovsky, Jia Deng, Hao Su, Jonathan Krause, Sanjeev Satheesh, Sean Ma, Zhiheng Huang, Andrej Karpathy, Aditya Khosla, Michael Bernstein, et al. Imagenet large scale visual recognition challenge. *International journal of computer vision*, 115:211–252, 2015. 1
- [95] Chitwan Saharia, William Chan, Saurabh Saxena, Lala Li, Jay Whang, Emily L Denton, Kamyar Ghasemipour, Raphael Gontijo Lopes, Burcu Karagol Ayan, Tim Salimans, et al. Photorealistic text-to-image diffusion models with deep language understanding. *Advances in neural information processing systems*, 35:36479–36494, 2022. 1
- [96] Axel Sauer, Dominik Lorenz, Andreas Blattmann, and Robin Rombach. Adversarial diffusion distillation. In *European Conference on Computer Vision*, pages 87–103. Springer, 2025. 7
- [97] Christoph Schuhmann, Romain Beaumont, Richard Vencu, Cade Gordon, Ross Wightman, Mehdi Cherti, Theo Coombes, Aarush Katta, Clayton Mullis, Mitchell Wortsman, et al. Laion-5b: An open large-scale dataset for training next generation image-text models. *Advances in Neural Information Processing Systems*, 35:25278–25294, 2022. 2
- [98] Uriel Singer, Adam Polyak, Thomas Hayes, Xi Yin, Jie An, Songyang Zhang, Qiyuan Hu, Harry Yang, Oron Ashual, Oran Gafni, Devi Parikh, Sonal Gupta, and Yaniv Taigman. Make-a-video: Text-to-video generation without text-video data, 2022. 1
- [99] Jascha Sohl-Dickstein, Eric Weiss, Niru Maheswaranathan, and Surya Ganguli. Deep unsupervised learning using nonequilibrium thermodynamics. In *International conference on machine learning*, pages 2256–2265. PMLR, 2015. 1
- [100] Jiaming Song, Chenlin Meng, and Stefano Ermon. Denoising diffusion implicit models. *arXiv preprint arXiv:2010.02502*, 2020. 1
- [101] Jiaming Song, Chenlin Meng, and Stefano Ermon. Denoising diffusion implicit models, 2022. 1
- [102] Qi Song, Qianyi Jiang, Lei Wang, Lingling Zhao, and Rui Zhang. Mugs: A multiple granularity semi-supervised method for text recognition. In *International Conference on Document Analysis and Recognition*, pages 173–188. Springer, 2023. 1
- [103] Yang Song and Stefano Ermon. Generative modeling by estimating gradients of the data distribution. In *Advances in neural information processing systems*, 2019. 1
- [104] Yang Song and Stefano Ermon. Generative modeling by estimating gradients of the data distribution, 2020. 1
- [105] Yang Song, Jascha Sohl-Dickstein, Diederik P Kingma, Abhishek Kumar, Stefano Ermon, and Ben Poole. Score-based generative modeling through stochastic differential equations. In *International Conference on Learning Representations*. 1
- [106] Yang Song, Jascha Sohl-Dickstein, Diederik P Kingma, Abhishek Kumar, Stefano Ermon, and Ben Poole. Score-based generative modeling through stochastic differential equations. *arXiv preprint arXiv:2011.13456*, 2020. 1
- [107] Jianlin Su, Murtadha Ahmed, Yu Lu, Shengfeng Pan, Wen Bo, and Yunfeng Liu. Roformer: Enhanced transformer with rotary position embedding. *Neurocomputing*, 568: 127063, 2024. 1, 3, 4
- [108] Keqiang Sun, Junting Pan, Yuying Ge, Hao Li, Haodong Duan, Xiaoshi Wu, Renrui Zhang, Aojun Zhou, Zipeng Qin, Yi Wang, et al. Journeydb: A benchmark for generative image understanding. *Advances in Neural Information Processing Systems*, 36, 2024. 7
- [109] Peize Sun, Yi Jiang, Shoufa Chen, Shilong Zhang, Bingyue Peng, Ping Luo, and Zehuan Yuan. Autoregressive model beats diffusion: Llama for scalable image generation. *arXiv preprint arXiv:2406.06525*, 2024. 1, 8, 4
- [110] Yu Sun, Shuohuan Wang, Shikun Feng, Siyu Ding, Chao Pang, Junyuan Shang, Jiaxiang Liu, Xuyi Chen, Yanbin Zhao, Yuxiang Lu, et al. Ernie 3.0: Large-scale knowledge enhanced pre-training for language understanding and generation. *arXiv preprint arXiv:2107.02137*, 2021. 1
- [111] Chameleon Team. Chameleon: Mixed-modal early-fusion foundation models. *arXiv preprint arXiv:2405.09818*, 2024. 4
- [112] Dreamina Team. Dreamina: Free ai image generator. <https://jimeng.jianying.com/>, 2023. 7
- [113] Gemini Team, Rohan Anil, Sebastian Borgeaud, Yonghui Wu, Jean-Baptiste Alayrac, Jiahui Yu, Radu Soriccut, Johan Schalkwyk, Andrew M Dai, Anja Hauth, et al. Gemini: a family of highly capable multimodal models. *arXiv preprint arXiv:2312.11805*, 2023. 1
- [114] Kolors Team. Kolors: Effective training of diffusion model for photorealistic text-to-image synthesis. *arXiv preprint*, 2024. 7
- [115] Wanxiang Team. Wanx. [urlhttps://tongyi.aliyun.com/wanxiang/](https://tongyi.aliyun.com/wanxiang/), 2023. 7

- [116] Keyu Tian, Yi Jiang, Zehuan Yuan, Bingyue Peng, and Liwei Wang. Visual autoregressive modeling: Scalable image generation via next-scale prediction. *arXiv preprint arXiv:2404.02905*, 2024. 1
- [117] Alexander Tong, Nikolay Malkin, Guillaume Hugué, Yanlei Zhang, Jarrid Rector-Brooks, Kilian Fatras, Guy Wolf, and Yoshua Bengio. Improving and generalizing flow-based generative models with minibatch optimal transport, 2023. 1
- [118] Hugo Touvron, Thibaut Lavril, Gautier Izacard, Xavier Martinet, Marie-Anne Lachaux, Timothée Lacroix, Baptiste Rozière, Naman Goyal, Eric Hambro, Faisal Azhar, et al. Llama: Open and efficient foundation language models. *arXiv preprint arXiv:2302.13971*, 2023. 1
- [119] Hugo Touvron, Louis Martin, Kevin Stone, Peter Albert, Amjad Almahairi, Yasmine Babaei, Nikolay Bashlykov, Soumya Batra, Prajwal Bhargava, Shruti Bhosale, et al. Llama 2: Open foundation and fine-tuned chat models. *arXiv preprint arXiv:2307.09288*, 2023. 1
- [120] Pascal Vincent. A connection between score matching and denoising autoencoders. *Neural computation*, 23(7):1661–1674, 2011. 1
- [121] Bram Wallace, Meihua Dang, Rafael Rafailov, Linqi Zhou, Aaron Lou, Senthil Purushwalkam, Stefano Ermon, Caiming Xiong, Shafiq Joty, and Nikhil Naik. Diffusion model alignment using direct preference optimization. In *Proceedings of the IEEE/CVF Conference on Computer Vision and Pattern Recognition*, pages 8228–8238, 2024. 2, 6
- [122] Xinlong Wang, Xiaosong Zhang, Zhengxiong Luo, Quan Sun, Yufeng Cui, Jinsheng Wang, Fan Zhang, Yueze Wang, Zhen Li, Qiying Yu, et al. Emu3: Next-token prediction is all you need. *arXiv preprint arXiv:2409.18869*, 2024. 8, 4
- [123] Ross Wightman. Pytorch image models. <https://github.com/rwightman/pytorch-image-models>, 2019. 6
- [124] Mitchell Wortsman, Peter J. Liu, Lechao Xiao, Katie Everett, Alex Alemi, Ben Adlam, John D. Co-Reyes, Izzeddin Gur, Abhishek Kumar, Roman Novak, Jeffrey Pennington, Jascha Sohl-dickstein, Kelvin Xu, Jaehoon Lee, Justin Gilmer, and Simon Kornblith. Small-scale proxies for large-scale transformer training instabilities, 2023. 2
- [125] Jinheng Xie, Weijia Mao, Zechen Bai, David Junhao Zhang, Weihao Wang, Kevin Qinghong Lin, Yuchao Gu, Zhijie Chen, Zhenheng Yang, and Mike Zheng Shou. Show-o: One single transformer to unify multimodal understanding and generation. *arXiv preprint arXiv:2408.12528*, 2024. 4
- [126] Jiazheng Xu, Xiao Liu, Yuchen Wu, Yuxuan Tong, Qinkai Li, Ming Ding, Jie Tang, and Yuxiao Dong. Imagereward: Learning and evaluating human preferences for text-to-image generation. *Advances in Neural Information Processing Systems*, 36, 2024. 2, 6
- [127] Zeyue Xue, Guanglu Song, Qiushan Guo, Boxiao Liu, Zhuofan Zong, Yu Liu, and Ping Luo. Raphael: Text-to-image generation via large mixture of diffusion paths. *Advances in Neural Information Processing Systems*, 36, 2024. 1
- [128] An Yang, Baosong Yang, Binyuan Hui, Bo Zheng, Bowen Yu, Chang Zhou, Chengpeng Li, Chengyuan Li, Dayiheng Liu, Fei Huang, et al. Qwen2 technical report. *arXiv preprint arXiv:2407.10671*, 2024. 1
- [129] Zhilin Yang. Xlnet: Generalized autoregressive pre-training for language understanding. *arXiv preprint arXiv:1906.08237*, 2019. 1
- [130] Jiahui Yu, Xin Li, Jing Yu Koh, Han Zhang, Ruoming Pang, James Qin, Alexander Ku, Yuanzhong Xu, Jason Baldridge, and Yonghui Wu. Vector-quantized image modeling with improved vqgan. *arXiv preprint arXiv:2110.04627*, 2021. 1
- [131] Jiahui Yu, Yuanzhong Xu, Jing Yu Koh, Thang Luong, Gunjan Baid, Zirui Wang, Vijay Vasudevan, Alexander Ku, Yinfei Yang, Burcu Karagol Ayan, et al. Scaling autoregressive models for content-rich text-to-image generation. *arXiv preprint arXiv:2206.10789*, 2(3):5, 2022. 1, 8, 4
- [132] Lijun Yu, Yong Cheng, Kihyuk Sohn, José Lezama, Han Zhang, Huiwen Chang, Alexander G Hauptmann, Ming-Hsuan Yang, Yuan Hao, Irfan Essa, et al. Magvit: Masked generative video transformer. In *Proceedings of the IEEE/CVF Conference on Computer Vision and Pattern Recognition*, pages 10459–10469, 2023. 1
- [133] Lijun Yu, José Lezama, Nitesh B Gundavarapu, Luca Versari, Kihyuk Sohn, David Minnen, Yong Cheng, Vignesh Birodkar, Agrim Gupta, Xiuye Gu, et al. Language model beats diffusion-tokenizer is key to visual generation. *arXiv preprint arXiv:2310.05737*, 2023. 1
- [134] Sihyun Yu, Sangkyung Kwak, Huiwon Jang, Jongheon Jeong, Jonathan Huang, Jinwoo Shin, and Saining Xie. Representation alignment for generation: Training diffusion transformers is easier than you think. *arXiv preprint arXiv:2410.06940*, 2024. 1
- [135] Biao Zhang and Rico Sennrich. Root mean square layer normalization, 2019. 2
- [136] Chunting Zhou, Lili Yu, Arun Babu, Kushal Tirumala, Michihiro Yasunaga, Leonid Shamis, Jacob Kahn, Xuezhe Ma, Luke Zettlemoyer, and Omer Levy. Transfusion: Predict the next token and diffuse images with one multi-modal model. *arXiv preprint arXiv:2408.11039*, 2024. 4, 19
- [137] Le Zhuo, Ruoyi Du, Han Xiao, Yangguang Li, Dongyang Liu, Rongjie Huang, Wenze Liu, Lirui Zhao, Fu-Yun Wang, Zhanyu Ma, et al. Lumina-next: Making lumina-t2x stronger and faster with next-dit. *arXiv preprint arXiv:2406.18583*, 2024. 1, 4